5

Processing and properties of inorganic nanomaterials

5.1 INTRODUCTION

Materials science is concerned to a great extent with the interaction between phenomena operating on different levels of scale, from that of the atom through to the macroscopic scale of everyday engineering components. For the majority of the time, however, materials science focuses on the intermediate scale; that of the microstructure, its means of production and control and properties related to it. We usually take microstructure to describe structural features on the scale between about 0.3 nm and 1 m and to include, in the classical definition, composition, crystal structure, grain size and shape (morphology), spatial distribution of phases, etc. The properties exhibited by a material depend, to a great extent, on the scale of the microstructure or, to be more specific, the relationship between microstructural scale and its influence in constraining particular physical mechanisms. For example, the strength of material is very strongly dependent on the grain size at all length scales, the grain boundary acting to constrain the propagation of dislocations through the material. In magnetic materials the interaction of the grain boundary with the domain wall thickness is of central importance. In both of these examples there exists a characteristic length; i.e., the critical bowing radius for dislocation propagation in the first example and the magnetic exchange length in the second, defining the scale on which the phenomena operate. When the constraints imposed by microstructure and these characteristic length scales overlap, it is quite often found that well-known laws governing material properties at conventional length scales break down or require re-examination. This is the range in which the new class of nanomaterials reside. As discussed in Chapter 1, the term 'nanomaterial' is taken as a descriptor for any material with at least one dimension smaller than 100 nm. Another way of defining the nanostructured regime is to state that a nanostructured material is attained when the

Nanoscale Science and Technology Edited by R. W. Kelsall, I. W. Hamley and M. Geoghegan

grains become equal to or smaller than those characteristic length scales related to their specific functionality. Control and manipulation of physical, mechanical and chemical properties as a function of the material microstructure on the nanometre scale often leads to the discovery of new materials, be they metallic, ceramic or polymeric in nature.

With the recent surge of interest in nanostructured materials, or to be more specific, the chemical, electronic and optical properties of nanomaterials, there is now a strong driving force to develop methods for their large-scale manufacture. Since the material properties of interest are very dependent on grain size, most applications will require the production of materials with well-controlled grain sizes and grain size distributions.

In this chapter we shall address the issues faced when processing inorganic nanocrystalline materials, the factors influencing their production and those governing the retention of nanostructure during further processing, and we shall briefly examine some of the interesting novel properties that are generated. The chapter could easily be retitled 'Processing *for* Properties in Inorganic Nanomaterials', as this is in fact our ultimate aim – the retention of the remarkable physical and chemical properties exhibited by materials on the nanoscale after processing to give useful engineering components.

5.1.1 Classification

The classification of bulk nanostructured materials is essentially dependent on the number of dimensions which lie in the nanometer range. Thus, depending on which dimensions fall within this range, they may be classified as: (a) zero-dimensional (0D); e.g., nanopores and nanoparticles; (b) one-dimensional (1D); e.g., layered or laminate structures; (c) two-dimensional (2D); e.g., filamentary structures where the length is substantially greater than the cross-sectional dimensions, and finally (d) three-dimensional (3D); e.g., structures typically composed of consolidated *equiaxed* (all three dimensions equally nanoscale) nanocrystallites. The classification system is useful in describing the type of structure we can manufacture. Figure 5.1 schematically illustrates all four types and, of these four types, 3D and 1D have so far received the greatest attention.

5.2 THE THERMODYNAMICS AND KINETICS OF PHASE TRANSFORMATIONS

5.2.1 Thermodynamics

Material microstructures are almost always unstable from a thermodynamic standpoint. That is, there is almost always some way in which the structure of a material can change to reduce the total energy. Because we strive to produce materials with structures that are optimised for specific applications, these changes will inevitably lead to deterioration in performance. This lack of thermodynamic stability is, however, often

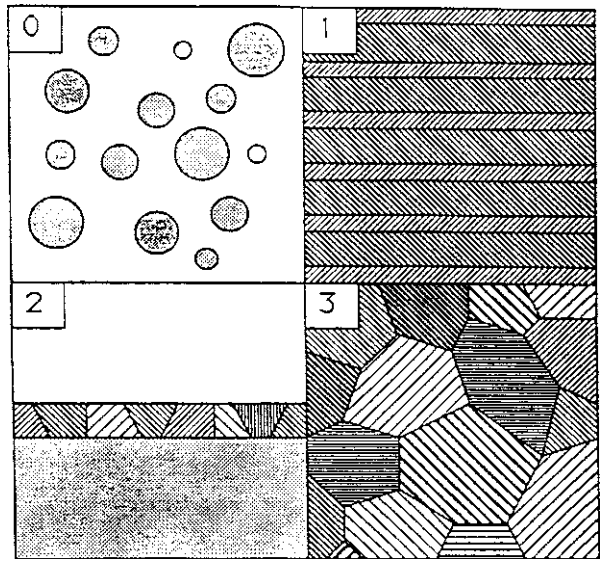

Figure 5.1 Schematic illustration of nanomaterials showing fine structural scale in different numbers of dimensions. These may be zero-dimensioned powders; thin deposited layers showing fine scale in one dimension; surface coatings with two-dimensional nanostructures; and three-dimensional nanostructures. Reprinted from *Nanostructured Materials*, Vol. 3, R. W. Siegel, Nanostructured Materials – Mind over Matter, pp. 1–18, copyright 1993, with permission from Elsevier

mitigated by very slow transformation kinetics which effectively impart an acceptable degree of stability.

Thermodynamic instability comes in two forms: genuine instability and metastability. Metastable structures must pass through an intermediate state of higher energy before a system can achieve the most stable state, thermodynamically speaking; i.e., that with the lowest energy. This necessitates that activation energy be supplied to the system before the reaction can take place, thereby lending a degree of 'stability' to the metastable state. In the case of genuine instability, however, no such activation barrier exists, with the result that the transformation is spontaneous.

In this chapter we are concerned with instability as related, for example, to the transformation from the liquid or vapour phase to the solid under favourable conditions, and structural metastability, which is particularly acute for nanostructured materials as a result of the excess energy associated with grain boundaries and interfaces. The distinction drawn between unstable and metastable transformations is due to Gibbs, and reactions are classified as being Gibbs type I or Gibbs type II transformations. For a Gibbs type I transformation, an energy barrier exists which is related to the nucleation of a stable nucleus of a new phase within the old before this new lower-energy structure may grow. In this process of nucleation and growth, the activation energy barrier results from the presence of an interface between the different phases. This type of transformation is highly localised and is characterised by dramatic changes in atomic arrangements on a small scale.

In contrast, Gibbs type II transformations involve the gradual change from an unstable phase to a more stable form via a series of intermediate steps, each possessing a steadily reducing free energy. Gibbs type II transformations are unlocalised; the whole of the structure transforms simultaneously. The well-known spinodal decomposition of a solid solution (Section 8.6.1) is perhaps the best-known example of this type of transformation.

Both Gibbs I and Gibbs II transformations are thermally activated; that is, they require a thermal activation to facilitate the movement of atoms to allow them to progress. This requirement means that at low temperatures the rate of change will be almost imperceptible; the transformation rates being significant only when atomic diffusion becomes significant (i.e., between $0.3T_{\mathrm{m}}$ and $0.5T_{\mathrm{m}}$, where T_m is the melting point).

The extent to which a particular reaction is feasible is given by the Gibbs free enthalpy function, G, which is defined as

$$G = H - TS, \tag{5.1}$$

where H is the enthalpy, T the absolute temperature and S the entropy of a system. There will be a free energy change associated with any change to the system. If a system changes from an initial state (i) to a final state (f) at constant temperature as a result of a chemical or physical process, there is a free energy change $\Delta G = G_f - G_i$ given by

$$\Delta G = \Delta H - T\Delta S, \tag{5.2}$$

where ΔH and ΔS are the corresponding enthalpy and entropy changes in the system. Reactions occur spontaneously at constant temperature and pressure when ΔG is *negative* and a system will tend to lower its energy by every available route until no further reduction is possible. At this stage $\Delta G = 0$ and we say that the system is in equilibrium. If ΔG is *positive* then the reaction is not possible.

Because it is the sign of ΔG that determines whether a reaction will or will not occur, the entropy change, ΔS, may be negative during a phase transformation. For example, in a transformation from the liquid or vapour phase to the solid, although there are fewer configurations available to the solid state, the overall decrease in enthalpy as a result of the transformation more than compensates for this, and the overall ΔG for the transformation is negative.

To examine its practical implication, let us consider a very familiar phase transition, that of liquid to solid. Upon freezing, a liquid changes from a condition in which there is no long-range order to one in which every atom is associated with a position in a crystal lattice. This type of reaction is defined as a first-order transition; this means that at the point of transition the change in entropy, ΔS, is discontinuous, leading to a discontinuous change in $\mathrm{d}G/\mathrm{d}T$. When a liquid turns into a solid at the freezing point T_{f}, a latent heat ΔH_{f} (also denoted L_V, the latent heat of fusion per unit volume) is released. Making the simplifying assumption that the enthalpy and entropy changes ΔH_{f} and ΔS_{f} do not change significantly as a function of temperature, this may be related to the change in entropy on freezing ΔS_{f} by

$$\Delta S_{\mathrm{f}} = \frac{\Delta H_{\mathrm{f}}}{T_{\mathrm{f}}} = \frac{L_v}{T_{\mathrm{f}}}. \tag{5.3}$$

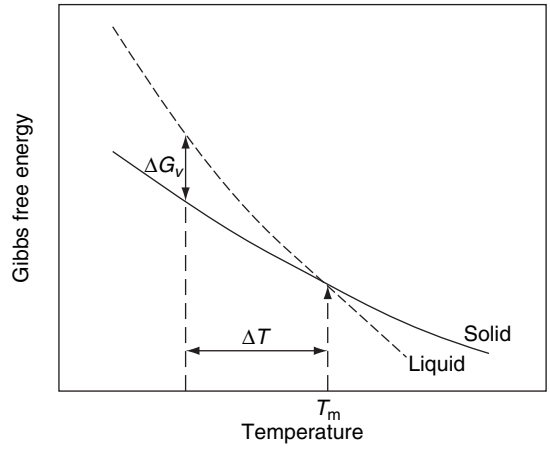

Figure 5.2 Schematic diagram of the variation of Gibbs free energy with temperature near the melting point T_m. At an undercooling ΔT the change in free energy per unit volume on transforming from the liquid to the solid state is ΔG_V

Figure 5.2 shows schematically how the free energy of a pure metal changes with temperature. At the equilibrium melting point, T_m, the free energies of the liquid and solid phases are equal. Below T_m, the solid has a lower free energy and is therefore the stable phase, whereas above T_m the reverse is true. The divergence of the free energy curves as the temperature falls below T_m, produces a steadily increasing driving force for crystallisation. The magnitude of the free energy change on crystallisation can be easily determined using this figure. In this case ΔG_v, the free energy driving the transformation at a small undercooling ΔT, is given by

$$\Delta G_v = \frac{L_v}{T_m} \Delta T \tag{5.4}$$

A sufficiently large free energy change will produce the driving force for nucleation of a new phase. This is the subject of the next section.

5.2.2 Homogeneous nucleation

For a phase transformation to occur there must be a nucleation event. This process is of vital importance to us in the understanding of the formation of nanostructured materials as the rate at which it occurs will influence the scale of the grain structure that is ultimately developed. The simplest models for nucleation are concerned initially with thermodynamic questions related to the formation of a single stable nucleus. After determining that nucleation may occur, we may then specify a nucleation rate, J, which is the number of stable nuclei forming per unit volume of liquid per unit time. At this point we move from the realm of thermodynamics to that of reaction kinetics. Ultimately, as we shall see in Section 5.2.5, it is these kinetics that will determine the structural scale.

Let us start by asking what energy is required to nucleate a spherical particle of radius r in an undercooled liquid. There will be a negative contribution to the free energy which is proportional to the volume of the sphere; this is because the solid phase has a lower free energy than the liquid at all temperatures below T_m, as discussed previously, and this will lower the free energy by an amount ΔG_V per unit volume. However, formation of a nucleus requires that an interface is produced; there is an interfacial energy between the solid (S) and liquid (L) phases γ_{SL} and this leads to a positive contribution to the free energy which is proportional to the surface area of the nucleus. We can represent the net change ΔG in the free energy on nucleating a droplet of radius r as

$$\Delta G = \frac{4}{3}\pi r^3 \Delta G_V + 4\pi r^2 \gamma_{SL}. \tag{5.5}$$

This function is sketched in Figure 5.3. By minimising the derivative of this free energy change with respect to r, we find a maximum at a critical radius r^*, given by

$$r^* = \frac{2\gamma_{SL}}{\Delta G_V}. \tag{5.6}$$

If a spherical cluster of atoms forms by some thermodynamic fluctuation, but has a radius less than r^*, it will be unstable, in that growth of such a cluster will increase the overall free energy of the system. If however the sphere is of size equal to or greater than r^* these particles will be stable and will grow, leading to a lowering of the system energy.

The energy required to form this critical nucleus ΔG^* may now be easily calculated; it is given by

$$\Delta G^* = \frac{16\pi\gamma_{SL}^3}{3\Delta G_V^2}. \tag{5.7}$$

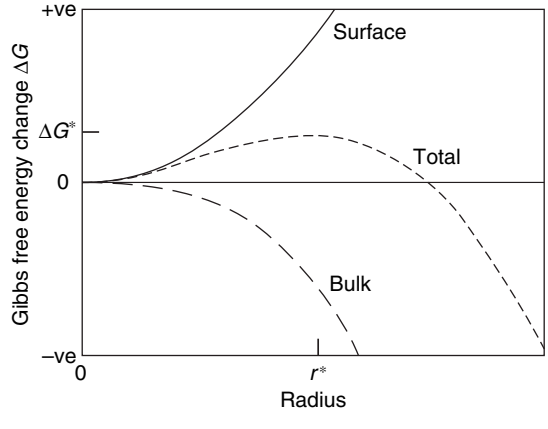

Figure 5.3 Schematic diagram of the variation in Gibbs free energy when a crystal of radius r is nucleated in a melt undercooled by ΔT below its melting point

Remembering from Section 5.2.1 that, for a small undercooling $\Delta T, \Delta G_V$ may be represented by

$$\Delta G_V = \frac{L_V \Delta T}{T_\mathrm{m}}, \tag{5.8}$$

where L_V is the latent heat of fusion per unit volume, we arrive at expressions for r^* and ΔG^* in terms of the undercooling:

$$r^* = \left(\frac{2\gamma_{\mathrm{SL}} T_\mathrm{m}}{L_V}\right)\frac{1}{\Delta T} \tag{5.9}$$

and

$$\Delta G^* = \left(\frac{16\pi\gamma_{\mathrm{SL}}^3 T_\mathrm{m}^2}{3L_V^2}\right)\frac{1}{\Delta T^2}. \tag{5.10}$$

Interestingly, these expressions show that the critical radius and the free energy barrier for nucleation decrease as the undercooling increases; nucleation becomes more likely under these circumstances.

Nucleation is an activated process; it can only occur if a thermal fluctuation occurs increasing the local free energy by an amount ΔG^*. The probability that such an event occurs is given by a Boltzmann factor, thus the rate of nucleation of droplets is proportional to

$$\exp(-\Delta G^*/k_\mathrm{B}T), \tag{5.11}$$

where the concentration of critical nuclei per unit volume C^* is given by

$$C^* = C_0 \exp\left(\frac{-\Delta G^*}{k_\mathrm{B}T}\right), \tag{5.12}$$

and C_0 is the number of atoms per unit volume.

The nucleation rate per unit volume, J, may then be obtained from the product of this concentration and the frequency of atom addition, f_0, to one such critical nucleus:

$$J = f_0 C_0 \exp\left(\frac{-\Delta G^*}{k_\mathrm{B}T}\right). \tag{5.13}$$

In the case of a liquid–solid phase transformation where atoms are being added by a diffusive mechanism, f_0 may be approximated by

$$f_0 = \frac{4\pi r^{*2} D_\mathrm{L}}{a^4}, \tag{5.14}$$

where D_L is the diffusivity in the liquid and a is the interatomic spacing.

Nucleation frequency, then, is a very strong function of temperature and also, via Equation (5.10) of ΔG^*, the undercooling; it changes from near zero to very high values over a very narrow temperature range. Using typical values, this equation predicts that significant rates will only be observed at significant undercoolings typically of the order of 0.2 T_m, yet we know from experience that crystals form at undercoolings of only a few degrees. This is because the theory outlined in this section describing homogeneous nucleation is relevant only to pure liquids and, as we shall see in the next section, the barrier for nucleation is greatly reduced by the presence of impurity particles, a substrate or indeed the walls of the vessel in which the material is placed. Such heterogeneous nucleation is, in practice, much more common than the homogeneous nucleation described here.

5.2.3 Heterogeneous nucleation

When a pre-existing surface or a solid particle is present in the undercooled liquid, this will reduce the activation energy required for the nucleation of a new crystal. This decrease can often be substantial, and in such cases the particle may act as a nucleation site.

Assuming for simplicity that the nucleus which forms on such a foreign body takes the form of a hemispherical cap as shown in Figure 5.4, the relationship between the contact angle, θ, and the interfacial tensions acting on the nucleus γ_{NS}, γ_{NL} and γ_{SL} between nucleant and solid, nucleant and liquid, and solid and liquid, respectively, may be derived by balancing forces at the interface:

$$\gamma_{SL} \cos\theta = \gamma_{NL} - \gamma_{NS}. \tag{5.15}$$

In the case of heterogeneous nucleation the critical energy required to form a heterogeneous nucleus, ΔG^*_{Het}, is reduced by a geometrical factor, $f(\theta)$, which defines the efficacy of the particle as a nucleation site and is defined as

$$f(\theta) = \frac{(1 - \cos\theta)^2(2 + \cos\theta)}{4}, \tag{5.16}$$

so that ΔG^*_{Het} becomes;

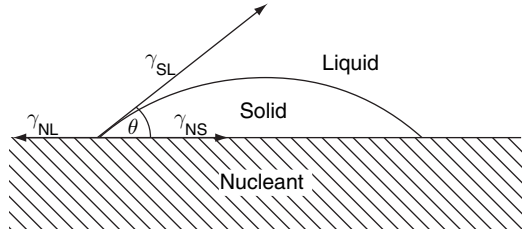

Figure 5.4 Heterogeneous nucleation of spherical cap on a solid surface which acts as a catalyst for crystallisation by lowering the activation energy for nucleation

$$\Delta G^*_{\text{Het}} = \left(\frac{16\pi\gamma_{\text{SL}}^3 T_{\text{m}}^2}{3L_V^2}\right)\frac{1}{\Delta T^2} f(\theta). \tag{5.17}$$

Thus, for all contact angles less than 90°, this factor substantially decreases the degree of undercooling required to achieve a measurable nucleation frequency. The most effective nucleation sites are seed crystals of the desired phase, as the contact angle is effectively zero.

This is the principle employed in the refinement of as-cast microstructures in conventional alloys. In this case nucleant particles, termed grain refiners, are deliberately added to increase the nucleation frequency, hence reducing the grain size. This method does not normally allow us to refine structures to below the micron scale; however the concept is useful in understanding those factors influencing formation of nanostructures by devitrification of metallic glasses and we shall come across them again in a later section.

5.2.4 Growth

Beyond the critical nucleus size r^*, atomic addition to the nucleus causes a continuous decrease in the free energy of the system. This means that growth of these post-critical nuclei, or clusters, is spontaneous. The rate of growth is controlled both by interfacial attachment kinetics and by the rate of transport of atoms to the interface of the growing crystallite.

At a growing crystal interface, atoms are continuously being attached and detached via thermally activated processes; the rates of attachment being independent of departure rate. Because there is a reduction in free energy when an atom attaches to an interface, departure is a more difficult process. The probability of the successful attachment of an atom to a growing interface is, however, dependent on the interfacial roughness.

At an atomically smooth interface (Figure 5.5(a)) an adsorbed atom from the liquid that establishes less than half of the atomic bonds that it would have in the bulk will have a low probability of being attached to the growing crystallite and will rapidly detach and return to the liquid. Growth in this case is difficult and relies on mechanisms whereby ledges are produced and propagated, as these are more favourable sites for atomic attachment. It may be demonstrated that the growth rate is proportional to the number density of active sites.

At an atomically rough interface (Figure 5.5(b)) where there are very large numbers of favourable sites for atomic addition, an atom joining from the liquid will make more

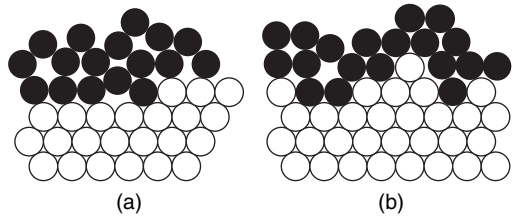

Figure 5.5 (a) Smooth and (b) rough solid–liquid interfaces: the black, liquid, atoms are restricted in terms of possible attachment sites in (a) whereas in (b) the number of possible attachment sites is high

than half the bulk atomic number of bonds and have a high probability of being incorporated into the growing crystal.

Although the example given here covers the basic concepts of crystallite growth, the actual growth mode and growth rate for a given material are very dependent on its method of synthesis and this is beyond the scope of this chapter. The interested reader should consult the bibliography at the end of this chapter for advanced study.

5.2.5 Overall transformation rate

The overall transformation rate df/dt, and hence the scale of the microstructure developed, will depend on both the nucleation frequency J and the growth rate R_G:

$$\frac{df}{dt} = f(J, R_G) \tag{5.18}$$

where f is the fraction of the whole that has been transformed. The coupling between these two processes depends on the microstructure and morphology of the structure being formed.

If we assume the transformation to be nucleated homogeneously, at small ΔT, transformation rates are controlled by the nucleation rate, since J is low and R_G is large. This condition results in large grains and coarse microstructures. When ΔT is high, transformation rates are controlled by the growth rate since J is large and R_G is low. This results in a fine-scale microstructure consisting of a large number of very small crystallites or grains. Intermediate to these extremes we would expect to see a situation where mixed control takes place.

If nucleation is heterogeneous, the situation is similar but these events will occur at lower undercoolings. If, however, heterogeneous nucleation occurs at very low undercoolings, all nucleation occurs prior to significant growth and the scale is determined to a great extent by the concentration of heterogeneous nucleants.

5.3 SYNTHESIS METHODS

Many of the techniques used in the synthesis of nanomaterials are basically those which have previously been employed in the manufacture of fine-grained and metastable materials. Modification and control of these processes has led to their being able to generate structures at the nanoscale and to facilitate this, it is vital that the underlying mechanisms responsible for the evolution of microstructure at a specific scale are well understood. For example, in the case of processes involving phase changes; e.g., from vapour or liquid to solid, control of the nucleation and growth kinetics is central to the control of the evolved microstructure. Processes involving the refinement of structure through application of mechanical work, on the other hand, may tend to a limiting minimum structural scale dependent on the maximum stresses that may be evolved during deformation and milling. This method can also be used to produce an intimate mix of particular compounds or elements, thereby allowing us to form nanoparticulate phases by chemical reaction via low-temperature heat treatments.

Synthesis of nanomaterials by all of these routes will be covered in what follows. Space dictates that only a very few of the multitude of synthesis techniques available for the preparation of nanomaterials can be covered in this chapter, yet those which are not covered explicitly are basically variations on the processes we do cover. We shall concentrate on techniques for producing bulk and particulate nanomaterials; techniques for the manufacture of thin films, wires and quantum dots have been covered in Chapters 1 and 3. The bibliography contains suggestions for further study.

5.3.1 Rapid solidification processing from the liquid state

Rapid solidification (RS) processes such as melt atomisation, melt spinning or planar flow casting and their derivatives all generate high cooling rates during solidification. The wide variety of rapid solidification methods available for the manufacture of non-equilibrium materials have been extensively reviewed on a number of occasions and several of these reviews are listed in the bibliography. In all of these RS processes, the liquid is manipulated such that at least one dimension is very small and in good thermal contact with a cooling substrate or fluid jet. The high cooling rates ($\sim 10^4$ K s^{-1} for atomisation and $\sim 10^6$ K s^{-1} melt spinning or planar flow casting) can lead to the formation of non-equilibrium microstructures, with metastable crystalline phases and metallic glasses being typical products.

The very large undercoolings obtained during RS mean that it is possible to generate nanostructured materials directly from the molten state; the nucleation rate being much enhanced and the growth rate suppressed. The latent heat evolved during nucleation and growth causes the temperature of rapidly solidified metals and alloys to increase from its maximum undercooled state. This phenomenon, termed recalescence, must be balanced by the rate of heat extraction if fine structures are to be generated by this technique. In practice this is difficult to achieve and the rise in temperature as a result of recalescence is often of sufficient magnitude to suppress further nucleation events, and hence it leads to the generation of relatively coarse microstructures. Whilst possible then, it is, generally speaking, quite difficult to control. Much greater control may be exercised if nanostructured alloys are derived from rapidly solidified precursors such as amorphous, or glassy, alloys by devitrification.

5.3.2 Devitrification

Controlled crystallisation, or devitrification, of amorphous alloys is a more convenient way of generating a nanostructured configuration than by direct quenching from the liquid state. Comparison of structures produced directly from the melt and those produced by devitrification show that there are no discernible differences between them. During conventional solidification the process is driven by an undercooling of only a few kelvins. Glassy or amorphous alloys, on the other hand, may be considered as deeply undercooled liquids when analysing the nucleation and growth kinetics. The transformation kinetics in this case are sufficiently slow, because of the much slower diffusion rates in the solid, that recalescence effects are negligible. Control of the crystallisation temperature remains critical, however. Glass-forming alloys are multicomponent systems; i.e., they

are usually composed of more than two elements, meaning that additional factors such as solute redistribution must be taken into account when analysing nucleation and growth.

Certain factors have been identified as promoting devitrification on a fine, but not necessarily nanometre, scale: the crystallising phase should have a composition distinct from the amorphous precursor; the presence of a very fine dispersion of precipitated phases or quenched-in nuclei which may act as heterogeneous nucleation sites; the alloy should exhibit a tendency to undergo a phase separation prior to crystallisation. The relative rates of nucleation and growth are, as with all other processes, also important to the scale of the structure produced.

The excellent soft magnetic properties generated by devitrification of the FINEMET materials have been a key driving force in the study of devitrification as a route to nanostructured alloys. The composition is basically an FeSiB glass-forming alloy to which small amounts of Cu and Nb have been added, Cu to stimulate nucleation and Nb to suppress crystallite growth. The role ascribed to Cu was for a long time purely speculative and based on the knowledge that the Fe–Cu binary system has a miscibility gap in the liquid state.

It was generally supposed that Cu clusters, approximately 5 nm in diameter, would spontaneously appear in the fully amorphous matrix during the earliest stages of a devitrification heat treatment and that these would promote nucleation of the ferromagnetic α-Fe nanocrystallites. This could be achived either by local depletion of Cu from the glassy matrix or by acting as *heterogeneous nucleation sites* (Section 5.2.3). This process is shown schematically in Figure 5.6. The assumption that Cu clusters serve as heterogeneous nucleation sites for the primary crystals seems quite reasonable, but direct proof that this was indeed the mechanism was not easy to obtain. Studies conducted using atom probe field ion microscopy (APFIM) finally delivered such proof. The rejection of Nb and B during growth leads to an enrichment in the remaining amorphous phase, which becomes stabilised and contributes to approximately 20% of the total volume of material. The alloy is therefore not fully nanocrystalline, but is a nanocomposite consisting of grains of diameter ~10 nm separated by ~2 nm of a glassy

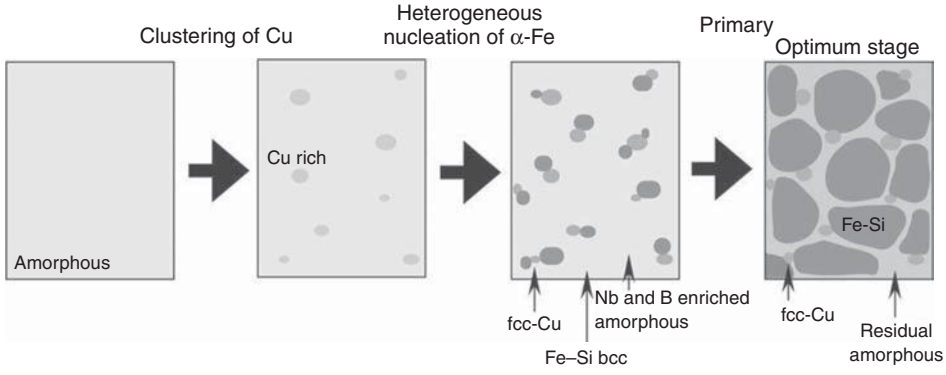

Figure 5.6 Schematic illustration of the microstructural evolution in melt-spun $Fe_{73.5}Si_{13.5}B_9Nb_3Cu$ amorphous alloy by primary crystallisation. Reprinted from *Progress in Materials Science*, Vol. 47, K. Hono, Nanoscale microstructural analysis of metallic materials by atom probe field ion microscopy, pp. 621–729, copyright 2002, with permission from Elsevier

matrix. The matrix further retards growth of the nanocrystals but also performs a crucial role in defining the magnetic properties (Section 5.8.2). Quenched-in nuclei, when present, fulfil a similar role but are not nearly as efficient at refining the grain structure and their presence does not guarantee the formation of a nanocrystalline structure. The miscibility gap responsible for the spontaneous formation of copper in the previous example may cause nanocomposite structures to form in a number of other alloy systems. Glasses based on palladium, copper, zirconium and aluminium have all shown a tendency to phase separation prior to crystallisation to produce two distinct amorphous phases; crystallisation then initiates at the interface between the two amorphous phases. The small fluctuation wavelength of the phase separation acts to minimise the grain sizes generated in this manner.

At present, there is no simple link between glass formation and the potential of an alloy system to yield a nanocomposite structure on devitrification. What is clear, though, is that this method of using metallic glasses as starting materials in the formation of nanostructured alloys has great potential, particularly when considering bulk metallic glass formers as precursors for the manufacture of nanostructured components with the ability of these alloys to be cast or warm forged to shape prior to devitrification being of particular interest.

5.3.3 Inert gas condensation

The inert gas evaporation–condensation (IGC) technique, in which nanoparticles are formed via the evaporation of a metallic source in an inert gas, has been widely used in the synthesis of ultrafine metal particles since the 1930s. A similar method has been used in the manufacture of carbon black, an ink pigment, since ancient times. The technique employed now for the formation of nanopowders, in reality, differs from that used to produce carbon and lampblack primarily in the choice of atmospheric composition and pressure and in the use of a chemically reactive source. Thus, although the technology is old, the application to the production of truly nanoscaled powders is relatively recent.

A schematic representation of a typical experimental apparatus for the production of nanopowders by IGC is shown in Figure 1.26. In its basic form, the method consists of evaporating a metallic source, using resistive heating (although radio frequency heating or use of an electron or laser beam as the heating source are all equally effective methods) inside a chamber which has been previously evacuated to about 10^{-7} torr and backfilled with inert gas to a low pressure. The metal vapour migrates from the hot source into the cooler inert gas by a combination of convective flow and diffusion and the evaporated atoms collide with the gas atoms within the chamber, thus losing kinetic energy. Ultimately, the particles are collected for subsequent consolidation (i.e., compaction and sintering, see Section 5.6), usually by deposition on a cold surface. Most applications of the inert gas condensation technique carry this approach to extremes by cooling the substrate with liquid nitrogen to enhance the deposition efficiency. Particles collected in this manner are highly concentrated on the deposition substrate. While the particles deposited on the substrate have complex aggregate morphology, the structure tends to be classified in terms of the size of the crystallites that make up these larger structures. The scraping and compaction processes take place within the clean environment to ensure powder surface cleanliness (i.e., to reduce oxide formation) and to minimise problems associated with trapped gas.

Although the IGC process generates a very narrow particle size distribution of 3D primary crystallites, typically a few nanometres in diameter, the exact size of the crystallites is very dependent on the type of carrier gas used, its pressure, the evaporation temperature and the distance between source and collecting position. Reducing the gas pressure and lowering the evaporation rate of the source and employing a light gas in the chamber produces a finer particle size. This effect is amplified by using He, which has a very high thermal conductivity. Higher evaporation temperature, inert gas pressure and inert gas molecular weight favours the formation of larger particles. The influence of the most important factors influencing the nucleation and growth of particles during IGC processing will be considered in the following sections.

5.3.3.1 Factors influencing nucleation and growth of fine particles

Nucleation kinetics

The production of fine particles requires that a high nucleation rate is achieved in the vapour whilst restricting the growth rate of these particles and preventing their coalescence. These requirements are conflicting.

In the case of a phase transformation involving homogeneous nucleation from a vapour phase, the volume free energy term is given by

$$\Delta G_V = \frac{RT}{V_m} \ln \Omega, \tag{5.19}$$

where R is the universal gas constant (8.314 J $K^{-1}mol^{-1}$), V_m is the molar volume and Ω is the vapour supersaturation, defined as the ratio (P/P_e) where P is the vapour pressure of the element present in the gas and P_e is the vapour pressure in equilibrium with the solid phase at temperature T (K). Using this expression for ΔG_V in Equations (5.5) to (5.14) shows that the critical free energy for nucleation, hence the nucleation frequency of atom clusters from the vapour, are very strongly dependent on the degree of vapour supersaturation. As the metal vapour is convected away from the evaporation source, the dilution of the metallic vapour by inert gas will lead to a decrease in the partial pressure from the saturation condition at the source, seemingly reduction ΔG_V. However, the much more rapid decrease in the equilibrium vapour pressure as the temperature rapidly decreases will more than offset this, resulting in a high vapour supersaturation to drive the homogeneous nucleation process.

At high supersaturations the initial nucleation frequency, J, may be extremely high, leading locally to a swift depletion of metal atoms from the vapour. This has implications for further growth of the particles by condensation, as we shall see in the next section.

Particle growth

Growth by condensation from the vapour

In the case of condensation from the vapour, the growth rate is proportional to the net difference in condensation and evaporation of atoms from the critical nucleus.

The driving force for growth is given by the difference between the instantaneous vapour pressure and the equilibrium pressure local to the growing cluster. The growth rate is therefore

$$\frac{dr}{dt} = \xi V_c \frac{P - P_e}{\sqrt{2\pi M k_B T}}, \tag{5.20}$$

where ξ, the condensation coefficient, is related to the number and nature of attachment sites and varies between 0 and 1, V_c is the molar volume of the condensate and M is the molecular weight of the inert carrier gas.

Any decrease in vapour supersaturation, (P/P_e), will therefore also produce a decrease in the driving force, $(P - P_e)$, for growth. Under ideal conditions the particles will be rapidly transported away, or advected, from the nucleation zone above the source in order to restrict their growth. They will then be deposited as a loosely agglomerated nanopowder at a collector.

The main growth mechanism for nanopowders may not, however, be condensation from the vapour. Alternative mechanisms of particle growth during the synthesis of nanopowders by evaporation or condensation methods, namely coalescence and agglomeration, may be the dominant growth processes.

Growth by coalescence and agglomeration

When the concentration of nuclei above the source is very high, particles may collide. The frequency at which these collisions occur is a function of the particle density per unit volume of gas, the particle diameter and the diffusion coefficient for the powder particle in the gas which is, obviously, dependent on the temperature. The rate of coalescence, on the other hand, is proportional to the diameter of the colliding particles and their viscosities. These also exhibit strong temperature dependences.

When the particles are very small and the gases still relatively hot, they will coalesce quickly after the initial collision, resulting in the formation of larger particles with a smaller surface area. At lower T the collision rate is greater than the rate of coalescence, and if there is still sufficient thermal energy to drive diffusive processes, this results in the formation of fractal-like agglomerates consisting of small nanocrystallites (Section 5.6.2). Although, in this instance, the fine nanometric structure of the colliding particles may still be preserved, the resulting agglomerates are actually much larger and may be quite rigid. These particles will have a large surface area.

The strength of the bonds which form between the nanoparticles in agglomerates may vary widely depending on material properties, gas atmosphere, and the temperature–time history that the particle has experienced. They may be soft, van der Waals type bonds or solid connections in the form of small necks which will give rise to hard, sintered agglomerates. Soft agglomerates, being formed at temperatures too low for significant coalescence, may be separated into their component nanocrystallites with relative ease, thus facilitating subsequent consolidation. Consolidation of powders containing hard agglomerates, on the other hand, is much more problematic and their presence frequently results in consolidates with densities well below the theoretical maximum (Section 5.6).

5.3.3.2 Improving yield, powder quality and production rate

The IGC process is relatively inefficient, as a result of powder condensation on the chamber walls, and the production rate is low. Moreover, the process as it now stands is batch based. Modification of the process to simultaneously increase the number concentration of nanoparticles produced and decrease the average particle size would seem to be in order if the process is to be scaled up to large volume manufacture of nanopowder.

The most obvious way of improving yield would appear to be to increase the evaporation rate from the source. Unfortunately, this has the effect of increasing the number of clusters within the nucleation zone, hence increasing the probability of interparticle collision and therefore the formation of agglomerates or large coalesced particles. If, however, enhanced evaporation of the source could be coupled with a more efficient method than free convection for transporting the powders away from the nucleation zone, this could lead to a significant improvement in terms of process efficiency and flexibility, with respect to product size, as well as increased material production rates.

The aerosol-flow condenser is a technique which has grown from this line of reasoning. In this jets of a carrier gas flow over an evaporation source, carrying away metal vapour. As the mixture of vapour and carrier gas flows downstream and cools, particles form and grow by the processes of nucleation, condensation and coagulation in a continuous process. By control of evaporation rate and gas flow rates, the cooling rate of the aerosol (the mixture of gas and particulate) may be varied to limit the extent of coalescence and agglomeration whilst simultaneously allowing greater control of the particle size and of the particle size distribution (PSD) generated.

5.3.4 Electrodeposition

The formation of nanoparticles and bulk nanostructured materials (BNMs) by electrodeposition; i.e., the deposition of a conductive material from a plating solution by the application of electrical current, may be achieved using either two separate electrolytes or, more conveniently, from one electrolyte by exercising appropriate control of the deposition parameters. These processes can be applied to the synthesis of pure metals, alloys and composites alike, have few size and shape limitations, and require only modest initial capital investment. Furthermore, and rather importantly from the point of view of its future potential as a synthesis route, the material production rate is high.

While many of the processes associated with the crystallisation from an electrolyte are, as yet, not well understood, it is clear that the electrodeposition of nanostructured materials is possible if a large number of nuclei form on the surface of the electrode and their growth is severely restricted. These requirements may be met by employing a variety of techniques either singly or in combination, including the use of high current density for a short duration, the use of organic additives as growth inhibitors, control of bath temperature, and manipulation of bath pH. The role of each of these factors in the control of microstructure evolution during electrodeposition will now be briefly examined.

5.3.4.1 Pulsed electrodeposition

Pulsed electrodeposition (PED) differs from the more normal direct current (DC) electroplating techniques in that the peak current density employed is very high (1–2 A cm^{-2}), much larger than that possible in DC electroplating, but that the duration of this high current density is very short. The deposition rate in the PED technique is governed by a number of controllable parameters, including the pulse duration, the time between pulses, and the pulse current. Cations are depleted from the electrolyte adjacent to the electrode during the application of the pulse and their levels are restored by the diffusive transport of material to this depleted region between pulses. The size of the nuclei is significantly dependent on both pulse duration and current density, whilst a balance must be struck between the replacement of cations close to the electrode by diffusion and the minimisation of grain coarsening when determining an appropriate interpulse time.

5.3.4.2 Growth inhibitors

Addition of suitable organic compounds to the electrolyte leads to the inhibition of grain growth. These adsorb on the electrodeposit, in a reversible way, and block active sites for growth, such as surface steps, hence leading to a reduction in the growth rate of crystallites. They also act to inhibit surface diffusion of adatoms, so that nucleation becomes the preferred method of electrolyte depletion. The crystallite size depends in this instance on the concentration of inhibitor in the electrolyte.

5.3.4.3 Bath temperature

At high temperature, adatom diffusion at the surface is much enhanced, thereby resulting in a much higher rate of grain growth. Inhibiting molecules also decrease in efficacy because the increased rate of desorption from growth sites as a result of the higher temperature will also increase the number of active attachment sites. On the other hand, reducing the bath temperature will contribute to the inhibition of growth. Changes in electrolyte temperature can also change the width of the grain size distribution as well as the average grain size.

5.3.4.4 Electrolyte bath pH

Control of the redox potential of the species by addition of a complex former which alters the redox of the desired species is particularly important if alloys with components of widely differing redox potentials are to be electrodeposited. If this equilibrium of the complexes depends additionally on the pH of the solution, a defined redox potential and therefore a defined alloy composition may be obtained by variation of the pH value.

5.3.4.5 Products

In addition to the obvious plating and surface coating of objects, nanostructured electrodeposits may be manufactured with complex geometries simply by altering the cathode shape. In a similar way, the process may also be modified to allow the production of different thicknesses of sheet or even powders.

The electrodeposition of nanostructures has an advantage over many other methods of synthesis in that it involves a logical extension of current industrial capability with respect to the commercial electroplating of materials. Nanomaterials can be manufactured easily using existing apparatus by a simple modification of bath chemistry and the plating methods used in current plating and electroforming operations. The industrial advantage of this method for the manufacture of fully dense nanomaterials via a one-step operation should not be underestimated.

5.3.5 Mechanical methods

5.3.5.1 Mechanical alloying or mechanical milling

Mechanical alloying (MA) or mechanical milling (MM) is a dry, high-energy ball milling technique. Strictly speaking, the term mechanical alloying is restricted to the formation of alloys or mixtures by mechanical means whereas mechanical milling is intended to describe the process of milling powders to reduce the particle size or for the refinement of structure. Since the original development of MA, as a way of incorporating oxide particles into nickel-based superalloys intended for application in gas turbines, it has been used in the preparation of a very wide range of materials from oxides to amorphous alloys and latterly, as MM, in the synthesis of nano-structured metals and alloys from atomised powders.

The technique is simple. Powders, typically 50 μm in diameter, are placed with hardened steel, ceramic or tungsten carbide (WC) balls in a sealed container and shaken or violently agitated. A high energy input is achieved by using a high frequency and small amplitude of vibration during milling; the collision time under these conditions is generally estimated to be of the order of 2 μs. There is a rise in the system temperature associated with such violent deformation but this is actually quite modest, typically 100–200 K.

Various ball mills are used to produce MA/MM powders, including tumbler mills, attritor mills, vibratory mills and planetary mills. They differ in capacity and milling efficiency but the process is effectively the same in each case. The simplicity of the apparatus allows it to be scaled up to the production of tonne quantities with relative ease and has the added advantage that both the starting materials and the product materials are in the form of relatively coarse ($\sim$50 μm) powders.

Problems inherent to the technique, such as contamination by reaction with the atmosphere or by wear of the milling medium and also the need to consolidate the powder product after synthesis without coarsening the nanostructure, are often used as arguments against implementing it as a method of nanostructured material production. Such contamination can, however, be minimised by limiting the milling time or by using

a protective milling atmosphere. Careful control of the processing conditions can also limit contamination by wear debris arising from the milling media to $\sim 1-2$ at% and oxygen and nitrogen levels for MA/MM materials can be less than 300 ppm. This, argue the proponents of the technique, is a higher purity of product than that achieved for materials synthesised by means such as IGC. In addition, the particle size of the product ($\sim 50\,\mu m$) means that there are fewer problems associated with porosity when consolidating than for true nanopowders.

In the case of nanostructured metals produced by mechanical milling, the structure is generated by the creation of a deformation substructure. During the initial stages of the milling process, a high dislocation density, ρ_d, is generated within each of the grains of the starting material as a result of repeated deformation by the milling medium. At a certain level of strain these dislocations start to annihilate and recombine, a process referred to as recovery, thereby reducing the overall dislocation density. The dislocations form loose tangles or networks which then evolve with increasing strain to produce low-angle grain boundaries (LAGBs) that separate individual subgrains. Each subgrain shows a small orientation difference or misorientation with respect to its neighbours. As the deformation proceeds, this misorientation increases by incorporation of further dislocations into the boundaries, causing them to gradually change in character, finally becoming high-angle grain boundaries (HAGBs). A high initial density of dislocations is therefore required to facilitate grain refinement by ball milling. It is through this process of continuous grain subdivision and dislocation accumulation in the boundaries that the observed three to four orders of magnitude reduction in grain size is achieved.

There is, however, a natural limit to the number of dislocations which may be present in a material. This limit is reached when the number of dislocations being produced by deformation and the number being annihilated by recovery are equal.

In metallic systems the grain size decreases with milling time, reaching a minimum grain size $\langle d \rangle_{min}$, characteristic for each metal. The minimum grain size that may be achieved during room temperature milling is found to vary roughly as the inverse of the absolute melting point, T_m, and also to be a function of the crystal structure of the metal. This is illustrated by Figure 5.7, which shows the variation of $\langle d \rangle_{min}$ with T_m for face-centred cubic (fcc) metals.

The present explanation for this behaviour is that, in metals with low melting points, the dislocation density is limited by recovery. Recovery is a thermally activated process, the activation energy for which is close to that for self-diffusion and it therefore scales with the alloy melting point (Section 5.5.1). In low melting point metals, recovery can be significant at room temperature and it is considered that it is this process which limits the final grain size rather than the deformation supplied by the mill. In contrast, for metals of high melting point such as the refractory metals, there will be almost no recovery at the milling temperature. The minimum grain size in this case is therefore limited by the stress required to generate and propagate new dislocations rather than the rate of recovery. The Hall–Petch equation (1.23) sheds some light on why a limiting value of grain size, generated by deformation, may occur. It is evident from Equation (1.23) that a decrease in $\langle d \rangle$ will give rise to an increase in yield strength and the most usual explanation of this relationship is based on a calculation of the stress ahead of a large array of dislocations piled up at a grain boundary. As shown in Figure 5.8(a),

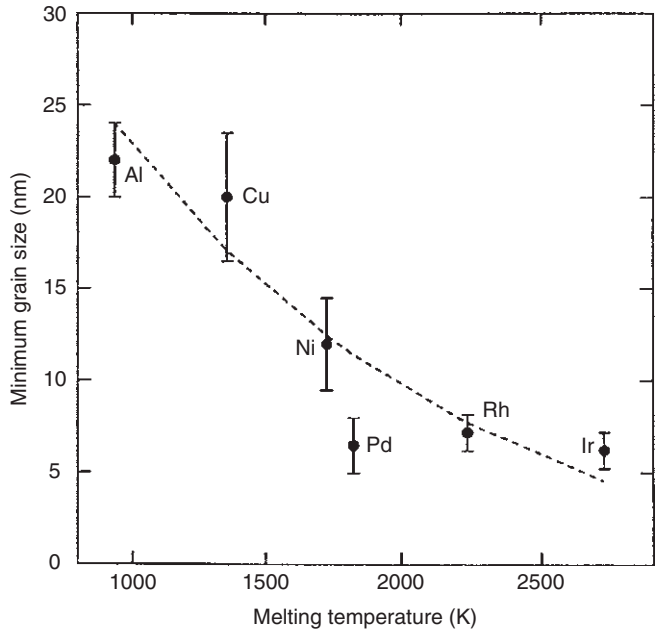

Figure 5.7 Minimum grain size obtained during mechanical milling for different fcc metals plotted against melting temperature. From J. Eckert, J. C. Holzer, C. E. Krill III and W. L. Johnson, *J. Mater. Res.* **7**, 1754 (1992)

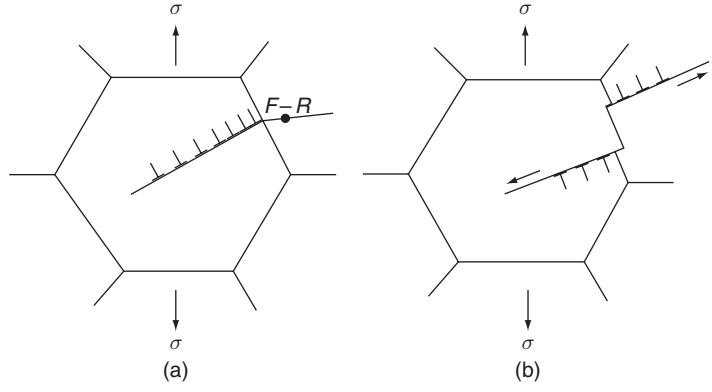

Figure 5.8 Two models proposed to explain the observed Hall–Petch behaviour in microcrystalline materials. F-R signifies a Frank-Reed type dislocation source is operating in this case. Details of both are given in the text: a) in this section and b) in section 5.7.1

the length of this pile-up can be assumed to be of the same magnitude as the grain size, d, and when the stress from the pile-up is large enough to induce plastic deformation in an adjoining grain, we say that the yield stress has been reached. If, during milling, a maximum deformation stress per collision, σ_{max}, can be generated, the Hall–Petch relation suggests that there exists a structural scale at which the material yield stress will

exceed this. At this value of $\langle d \rangle$, deformation will no longer proceed by the generation and propagation of matrix dislocations; the minimum grain size will then have been attained. This competition between the deformation and recovery behaviour is often cited as the reason for the generation of a characteristic $\langle d \rangle_{\min}$ for a given material.

Once an entirely nanocrystalline structure is formed, further deformation is accomplished by grain boundary sliding (GBS) and there is no further refinement of structural scale. GBS does, however, accommodate deformation energy; this is stored within the grain boundaries themselves and also in the form of strains within the nanograins which arise because of grain boundary stresses. Grain boundary energies may, as a result, be higher than expected, as much as 25% higher than the value for the grain boundary energy in a coarse-grained sample.

5.3.5.2 Mechanochemical processing

Mechanically activated exchange reactions have also been examined as possible methods for the synthesis of ultrafine and nanoscale powders. In this process, chemical precursors undergo reaction, either during milling or subsequent low-temperature heat treatment, to form a nanocrystalline composite consisting of ultrafine particles embedded within a salt matrix. The ultrafine powder is then recovered by removing the salt through a simple washing procedure. This process is termed mechanochemical synthesis and, to date, it has been successfully applied to the preparation of a very wide range of nanomaterials, including transition metals, magnetic intermetallics, sulfide semiconductors and oxide ceramics.

The technique is essentially equivalent to that for MA. In this process, however, the starting powders are typically in the form of reactant compounds. These are milled to form an intimate mixture of the reactants which either react during milling or during a subsequent low-temperature heat treatment, to yield a product and a by-product phase. Generally speaking, the product is finer if the reaction can be made to occur in a controlled manner during heat treatment.

The severe microstructural refinement imparted by the high-energy milling step, however, has the effect of decreasing the effective diffusion distance between the reactant phases. The net effect is that the chemical reactivity of the mixtures is increased, and if the energetics of the reaction is favourable, this will occur during the milling operation after a given milling time has elapsed.

To facilitate greater control of the reaction a diluent phase, usually the same compound as the reaction by-product, is often added to the milling mixture. This leads to a reduction in the overall frequency of reactant–reactant collisions during milling, thereby reducing the reaction rate and the rate of heat generation. The diluent also increases the diffusion distance between crystallites of the product phase, such that coarsening of the nanocrystallites during the heat treatment stage will be inhibited by its presence.

As with mechanical attrition, the process can be readily scaled up to the production of commercially viable quantities of nanopowder. Furthermore, the simultaneous formation of ultrafine particles with an intervening salt matrix suggests that agglomerate formation can more readily be avoided than is possible with other synthesis techniques since the salt matrix inherently separates the particles from each other during processing. The mechanochemical synthesis technique therefore allows significant control to be

exercised over the characteristics of the final washed powder. The method has significant potential for the low-cost synthesis of a wide range of ceramic and metallic nanopowders, including the production of UV absorbers such as ZnO and TiO_2 for the cosmetics industry. The unique combination of the band gap structure of these semiconducting oxides, which results in their absorbing strongly in the UV part of the spectrum, and the very fine scale of the powders, so that the particles do not strongly scatter incident light, make them excellent alternatives to organic based sunscreens.

5.4 STRUCTURE

The total intercrystalline region – grain boundaries (where individual grains meet to form an interface), edge length (lines where three grains meet) and vertices or triple points (higher-order junctions) – is important in the microstructure of a material at any length scale. Grain boundaries act as rapid diffusion routes and barriers to dislocation motion; grain corners and edges may act as nucleation sites for recrystallisation or may have mechanical properties different from those of the bulk. As the average grain size, $\langle d \rangle$, falls below 100 nm, however, the relative proportion, and hence the overall influence of these geometrical components of the microstructure on the material behaviour, increases dramatically. If the mean diameter of grains in the assembly is $\langle d \rangle$, then the number of grains per unit volume, N_V, is proportional to $1/\langle d \rangle^3$ and the mean grain boundary area A_V, mean edge length L_V and mean number of corners C_V per unit volume are given by:

$$A_V = C_A/\langle d \rangle, \tag{5.21}$$

$$L_V = C_L/\langle d \rangle^2, \tag{5.22}$$

$$C_V = C_C/\langle d \rangle^3, \tag{5.23}$$

where the constants C_A, C_L and C_C are dependent on the assumed grain geometry. In the case of a grain boundary of thickness δ (typically 0.5 nm), the volume fraction of atoms in the grain boundaries, F_V, is given by

$$F_V = C_A \delta/\langle d \rangle. \tag{5.24}$$

What is immediately obvious, however, from this expression is that F_V becomes important only as δ and $\langle d \rangle$ become comparable in size, and gains greater significance the closer they become to each other. In the case of nanomaterials, for example, the fraction of atoms per unit volume considered to be existing within the boundary changes very rapidly, varying from 0.03 when $\langle d \rangle$ is 100 nm to greater than 0.5 when $\langle d \rangle$ is 5 nm. The distance between atoms in the boundary is slightly altered with respect to that in the bulk and the structure is somewhat looser. This presence of such a high fraction of 'loose' structure has been employed in the explanation for the deviation of many properties of nanomaterials from those observed on the conventional scale. In some cases, however, as we shall see later in this chapter, the properties were later found to result from poor

compaction, the presence of defects or other causes related to processing, rather than as a result of structural relaxation effects.

In addition to the fact that grain boundaries are essentially non-equilibrium defects, such an excess of intercrystalline material makes nanomaterials thermodynamically unstable and provides a driving force for structural coarsening. It is of little surprise that the processing of nanomaterials is concerned, to a very great extent, with the suppression of grain growth.

5.4.1 Microstructure

5.4.1.1 Grain size and matrix strain

As stated, the grain size is the most important structural parameter in nanomaterials. The properties of nanomaterials depend on it and thus, an accurate method of determining grain size is of paramount importance. However, the uncertainty in grain size measurement for nanomaterials is much greater than for materials with conventional microstructural scale. As such, relationships for these materials derived directly from experimental data should be viewed with some caution.

There are a number of analytical techniques available to us for measuring grain size, microstrain and also the apparent nanoparticle size, including X-ray diffraction, transmission electron microscopy (TEM) techniques and measurement of specific surface area of nanopowders.

The width of the Bragg reflection in a standard X-ray diffraction pattern can provide information on the average grain size. The peak breadth increases as the grain size decreases, because of the reduction in the coherently diffracting domain size, which can be assumed to be equal to the average crystallite size. If the broadening arises entirely as a result of size effects, the full width at half maximum (FWHM) true peak breadth (corrected for instrumental broadening and measured in radians), β, is related to the average grain size $\langle d \rangle$ via the Scherrer equation:

$$\beta = \frac{0.9\lambda}{\langle d \rangle \cos\theta}, \tag{5.25}$$

where λ is the wavelength of incident X-ray radiation, and θ is the Bragg angle for the peak being analysed. The error in $\langle d \rangle$ obtained by this technique is of the order of 10%, meaning that it is difficult to measure small changes in grain size with great certainty. On the positive side, the measurement is simple to perform and the volume sampled is large compared with other techniques such as TEM. Peak breadth may also be influenced by the degree of microstrain and the peak breadth for an exclusively strain-broadened profile is approximately related to the root mean square strain, $\langle e^2 \rangle^{1/2}$, thus

$$\beta = k\langle e^2 \rangle^{1/2} \tan\theta, \tag{5.26}$$

where k is a constant depending on the strain distribution in the specimen. Where both size and strain components are present these may be separated. These methods are quite

involved and beyond the scope of this chapter, but several useful references are included in the bibliography for the interested reader.

TEM techniques are ideal for the direct measurement of grain size, grain size distributions and any structural non-uniformity such as a bimodal grain size distribution. This type of measurement is however, rather labour-intensive and a very large number of grain size measurements are needed before the results can be considered to be statistically significant. Nevertheless, it is a useful complementary technique.

5.4.1.2 Particle size measurement

The average particle size $\langle D \rangle$ of a nanopowder may be derived from a measurement of its specific surface area (area per unit mass), A_m, via the relation

$$A_m = \frac{6}{\rho_{\text{th}} \langle D \rangle}, \tag{5.27}$$

where ρ_{th} is the theoretical density of the material. This will give a value for the apparent particle size of a powder which may differ significantly from the nanocrystallite grain size derived by X-ray analysis.

Comparison of measured values of grain or particle size derived by different techniques is a good guide to the overall quality of a true nanopowder; close correlation between the results of different measurement techniques being indicative of a powder of good quality with respect to average particle size, size distribution and particularly the degree of particle agglomeration and coalescence.

5.4.2 Grain boundary structure

It has been proposed that the grain boundaries in nanomaterials are different in character from those in the same material in the coarse-grained condition. Those proposing these differences postulated that the boundaries between nanocrystallites might have unique characteristics resulting from the constraints imposed on the grain boundary atoms as a result of their synthesis by consolidation of nanopowders.

High-resolution TEM work has shown that there is in fact no difference in the type of grain boundary structures observed in nanomaterials when compared with the coarse-grained version of the same material produced by the same route. The low density of grain boundaries in consolidated nanopowders may therefore result from a high fraction of distributed nanoporosity. This issue remains unresolved.

5.4.3 Structural metastability

As well as the morphological metastability, nanomaterials may also exhibit additional topological metastabilities (e.g., as a result of a different crystal structure from that at equilibrium) or compositional metastabilities (e.g., as a result of the

occurrence of extended solid solubilities) which impart unusual and sometimes useful characteristics to the material. There are numerous reviews of the techniques and effects of the processing of metastable materials, most of which are related to rapid solidification (RS) processing. This chapter is concerned with factors influencing the retention of nanostructure, so these other forms of metastability, although important, are beyond its scope. A number of reviews are included in the bibliography for further study.

5.5 MICROSTRUCTURAL STABILITY

As discussed in Section 5.2, most useful engineering materials are metastable to a greater or lesser extent. Thus all may revert to a lower energy state if sufficient thermal energy is imparted to allow the activation barrier for this transformation to be overcome. Nanostructured materials are highly metastable, largely as a result of the enhanced number density of grain boundaries. The properties that engineers and scientists wish to exploit are, however, strongly dependent on the microstructural scale. The manufacture of useful components from nanomaterials often necessitates a consolidation step, and such consolidation processes normally require that the powders are exposed to relatively high temperatures. At these temperatures, when diffusion becomes significant, the nanograins may exhibit rapid rates of growth leading to an unacceptable coarsening of the structure, thereby returning the material properties to those of their coarse-grained counterparts.

This section discusses several phenomena of importance to the processing of nanomaterials, namely, diffusion, grain growth and pinning mechanisms. In the sections that follow their relevance to consolidation processing will also be considered.

5.5.1 Diffusion

Chemically driven atomic motion in crystalline materials is described by Fick's laws of diffusion. Fick's first law states that the mass flux per unit area J is proportional to the concentration gradient present in the material:

$$J = -D\frac{dC}{dt}. \tag{5.28}$$

Local conservation of material is expressed by the equation of continuity:

$$\frac{dC}{dt} = -\frac{dJ}{dx}. \tag{5.29}$$

Combining this with Equation (5.28) leads to Fick's second law:

$$\frac{dC}{dt} = D\frac{\partial^2 C}{\partial x^2} \tag{5.30}$$

The constant of proportionality in these equations, D, is defined as the diffusion coefficient and is itself governed by an Arrhenius-type expression:

$$D(T) = D_0 \exp\left[\frac{-Q_D}{RT}\right] \tag{5.31}$$

where D_0 is a pre-exponential factor and Q_D is the molar activation energy for diffusion. If this diffusion occurs by transport through the crystal lattice, we term this lattice or volume diffusion and the activation energy is denoted as Q_V.

Diffusion is, however, much more easily accomplished along surfaces and grain boundaries, or via dislocations, than through a lattice, because these features have a more open structure. This type of 'short circuit', grain boundary diffusion may also be well represented by Equation (5.31), where the pre-exponential term is now D_{B0} and the activation energy is for boundary diffusion, Q_B.

Where there is diffusion both through the lattice and via a high-diffusivity path, it is more appropriate to use an apparent diffusion coefficient, D_{eff}, which is given by the expression

$$D_{eff} = D_V + \frac{\delta}{\langle d \rangle} D_B, \tag{5.32}$$

where $\langle d \rangle$ is the average grain size and δ is the grain boundary width (taken to be $\sim 0.5\,\text{nm}$) in the case of grain boundaries acting as the high-diffusivity path. When diffusion is enhanced by the presence of these dislocations, the expression for D_{eff} is

$$D_{eff} = D_V + a_c \rho_d D_p, \tag{5.33}$$

where ρ_d is the dislocation density (with units m^{-2}), a_c is the area of the dislocation core associated with rapid diffusion (m^2), and D_p is the pipe diffusion coefficient.

From these expressions it is immediately obvious that grain boundary and dislocation pipe diffusion will dominate when the second term on the right-hand side of Equations (5.32) and (5.33) is greater at a given temperature than the lattice diffusion term. When the high-diffusivity path contribution to D_{eff} far exceeds that of lattice diffusion, the contribution of the lattice to the overall mass transport may be ignored.

It is found that, for a given crystal structure and bond type, the activation energy is approximately proportional to the melting temperature, and that the diffusion coefficient at the melting temperature and the pre-exponential factor, D_0, are approximately constant. Within each class and for each type of diffusion path, the diffusion coefficient exhibits the same relationship with respect to the absolute temperature T. In most close packed metals the activation energy for lattice diffusion and grain boundary diffusion may be approximated as $18RT_m$ and $10RT_m$, respectively with $D_0 = 5.4 \times 10^{-5}\,\text{m}^2\,\text{s}^{-1}$ and $\delta D_{B0} = 9 \times 10^{-15}\,\text{m}^3\,\text{s}^{-1}$; for bcc these activation energies are approximated by $18RT_m$ and $12RT_m$ with $D_0 = 1.6 \times 10^{-4}\,\text{m}^2\,\text{s}^{-1}$ and $\delta D_{B0} = 3.4 \times 10^{-13}\,\text{m}^3\,\text{s}^{-1}$.

Using these typical values we may deduce that the dominant mass transport mechanism for both crystal structures is indeed grain boundary diffusion for all $T \leq T_m$ when

$\langle d \rangle$ is less than 100 nm. In coarse-grained materials this tends to be the case only at lower temperatures, typically less than $0.5T_m$, where diffusion is, in any case, rather limited.

5.5.2 Grain growth

Grain growth occurs in polycrystalline materials to reduce the overall energy of the system by reducing the total grain boundary energy. Grain boundaries are a non-equilibrium defect; a single-phase material is most thermodynamically stable when all boundaries are removed. In nanomaterials, where the grain boundaries constitute a significant proportion of the total volume, this tendency for growth should be expected to be particularly strong and the main task during processing of nanomaterials is, as far as possible, to prevent this from happening.

If we assume that the mean curvature of boundaries in all grains in a polycrystalline aggregate to be inversely proportional to the average grain radius $\langle r \rangle$, then the mean driving force for growth is given by $\alpha\gamma_b/\langle r \rangle$, where γ_b is the grain boundary energy (usually assumed to be $\sim 1/3$ of the surface energy of the material γ_S) and α is a geometric constant (equal to 2 if the grains are considered to be spherical). Assuming that the grain boundary energy is isotropic (i.e., equal for all grain boundaries and in all crystallographic directions) and that the boundary velocity is proportional to this driving force, the average growth velocity of the grain assembly is given by

$$\frac{d\langle r \rangle}{dt} = \alpha \frac{\gamma_b}{\langle r \rangle}. \tag{5.34}$$

Integrating this expression gives the following relationship for grain growth as a function of time:

$$\langle r \rangle^2 - \langle r_0 \rangle^2 = Kt, \tag{5.35}$$

where K is given by

$$K = K_0 \exp\left(-\frac{Q_G}{RT}\right) \tag{5.36}$$

and Q_G is the activation energy for grain growth.

Thus, for the ideal case of an isotropic grain assembly consisting of equiaxed grains of radius $\langle r \rangle$, growth obeys a parabolic rate law. By determining the Arrhenius rate parameter K over a range of temperatures, the activation energy for grain growth, Q_G, may also be determined.

In practice, experimental data shows that grain growth can be described by a similar rate law expression, but that the observed behaviour is rarely parabolic. The general form of the expression for grain growth is therefore taken to be

$$\langle r \rangle^n - \langle r_0 \rangle^n = Kt, \tag{5.37}$$

where n is found to vary over a wide range and also to be a strong function of temperature.

At low normalised temperatures (T/T_m), n typically takes a high value, in common with conventional materials. n decreases towards 2, the theoretical value, as the annealing temperature increases towards the melting point. It is interesting to note that the values for the exponent show the same overall trend; i.e., tending to be high at low T/T_m and decreasing as T/T_m increases, irrespective of whether the material is metallic or ceramic, conventional or nanostructured. There are of course notable exceptions, such as n-Al_2O_3, where the exponent has been observed to be 4 at all T/T_m. Nevertheless, the general trend holds true.

This variation in the value of n occurs essentially because materials are non-ideal and, as the driving force for growth is in any case very small, any deviation from this idealised behaviour will exert a significant influence on the observed grain growth kinetics. In reality, grain assemblies may be non-equiaxed or there may be a wide grain size distribution present. Such departures from ideality may be responsible for the high values of n during the early stages of grain growth. It is also highly likely that there will be some degree of anisotropy and non-uniformity in the grain boundary energy, as nanoparticles may also exhibit faceting behaviour.

The activation energy for grain growth is, generally speaking, more difficult to determine reliably, particularly given the large deviation of n from ideality. However, to date, experimental studies have tended to show that the activation energies in a particular nanomaterial are very similar in magnitude to those for grain boundary diffusion. Here again, there are some notable exceptions, in particular nanocrystalline Fe, for which a low value is observed for low T/T_m ($125\,kJ\,mol^{-1}$), whereas a much higher value is obtained at high T/T_m ($248\,kJ\,mol^{-1}$). The higher value here is more representative of the activation energy for lattice diffusion and is similar to the value obtained for coarse-grained Fe, whereas the low-temperature value is actually smaller than expected for grain boundary diffusion in Fe.

That we have a metastable microstructure which is prone to coarsening is therefore not in doubt, and the issue that must be addressed is that of the retention of this nanostructure during subsequent processing (e.g., sintering and compaction) to form bulk materials.

5.5.3 Zener pinning

To prevent growth of nanomaterials during processing, the motion of the grain boundaries must be impeded. This can readily be achieved via the pinning effect of fine pores or second-phase particles. We will call both of these impediments obstacles. Moving boundaries will become attached to these obstacles and they, in turn, will exert a retarding force on the boundary, proportional to the length of the boundary attached to them. The maximum force which may be exerted by a single particle on such a moving boundary is

$$F_{max} = \pi r_p \gamma_b, \tag{5.38}$$

where γ_b is the grain boundary energy and r_p is the obstacle radius. If the number of obstacles per unit volume is f_r, then the number of obstacles per unit area intersecting a randomly drawn plane is given by $3f_r/2\pi r_p^2$, and the retarding force per unit area of that plane is then approximated by

$$\frac{3f_r}{2\pi r_p^2}\pi r_p\gamma_b = \frac{3f_r\gamma_b}{2r_p}. \tag{5.39}$$

This force opposes the driving force for grain growth (5.34) so that, for growth to occur, the driving force must be greater than the retarding force; i.e.:

$$\frac{\alpha\gamma_b}{\langle r\rangle} > \frac{3f_r\gamma_b}{2r_p}. \tag{5.40}$$

In otherwords, there exists a critical ratio f_r/r_p above which no grain growth may occur. Thus, if such a stable dispersion of obstacles were to be introduced into a microstructure (a) by compaction to produce a fine distribution of pores, (b) by precipitation of a second phase or (c) by contamination from surface oxides, for example, then the scale of that microstructure could be stabilised. This will only succeed, however, if the particles present on the boundaries do not coarsen; coarsening would obviously lead to a change in the ratio f_r/r_p as a result of an increase in r_p, hence reducing the efficacy of pinning. Pinning may also, under certain conditions, lead to what is termed abnormal growth. This occurs when rapid coarsening of precipitates (i.e., the reduction in their number density and increase in the average pinning particle size) on some grain boundaries allows them to break free and move. In this situation a bimodal grain size distribution is rapidly established in which very large grains are surrounded by, and are growing into, fine-grained regions. Therefore care must be taken to select a suitable pinning phase when employing this effect.

5.5.4 Solute drag

A second commonly used retarding effect is that of solute drag. The degree to which a solute segregates to a grain boundary is inversely related to the solid solubility of that element in the matrix. The solute drag effect is, however, quite a complex phenomenon; at low boundary velocities the drag force is inversely proportional to the solute concentration at the boundary whilst, when the solute concentration is low or there is an increased driving force for growth, the solute can exert no net influence on the boundary mobility. The apparent activation energy for grain growth will also decrease as the temperature is increased since the effect of the solute is less pronounced at higher temperatures.

As the boundaries of nanomaterials exhibit higher solute atom solubility than those of coarse-grained materials, solute drag effects may be expected to be even more pronounced. A further possible influence of this enrichment is that it may lead to a significant decrease in the driving force for grain growth by reducing γ_b and thus, according to Equation (5.15), reducing the driving force for grain growth. A good example of this type of growth inhibition is that exhibited by nanocrystalline Cu–Bi. The very low solid solubility of Bi in Cu promotes its segregation to grain boundaries and the grain growth rate of Bi-doped nanocrystalline Cu is therefore much reduced in comparison to the non-doped nanocrystalline Cu. This effect has been attributed to the action of Bi in reducing γ_b. Similar strategies are also effective in the retention of ceramic nanostructures, for example the low-level doping of TiO_2 by yttrium has been found to be useful in retaining sub-100 nm grain sizes during sintering.

There are, however, some some negative aspects to adopting doping and solute drag strategies for retaining fine grain sizes. Their presence may for example be highly detrimental to properties (e.g., mechanical, magnetic or catalytic) and, as with all processing, this must be considered when designing the material composition and selecting the most suitable processing route.

5.6 POWDER CONSOLIDATION

Techniques employed to date in the consolidation of nanopowders to form bulk nanostructured materials (BNMs) have been borrowed, to a large extent, from the powder metallurgical and ceramic processing industries. However, because of the very small size of the powder particles, special precautions must be taken to reduce the interparticle friction, and hence heating, and also their activity, to minimise the danger of explosion or fire.

Close control of the consolidation stage is essential to the scientific study of nanomaterial properties and to their use in engineering applications. A number of apparently remarkable changes in mechanical and magnetic properties of materials attributed to the nanoscale structure during the early stages of nanomaterial development were later found to be a processing artefact. A good example is the Young's modulus of elasticity, E, which was initially thought to be significantly lower for nanomaterials than for those same materials at conventional grain sizes. It is now almost universally accepted that this observation was entirely attributable to the presence of extrinsic defects such as pores or cracks which occurred during the consolidation stage of processing. This example highlights the greatest problem associated with the study of the properties of nano-materials – the production of high-quality, fully dense BNMs. The consolidation stage need not be viewed in such negative terms, however, as at this stage we may chose to combine different nanopowders to form composites, either directly by the combination of desired phases in desired quantities or by mixing precursor nanopowders and promoting reactions by subjecting these mixtures to heat treatment under controlled conditions.

The various stages of the consolidation process will be considered briefly here. In addition, novel sintering techniques that have been applied to nanomaterial consolidation and comment on their potential for exploitation will be briefly considered. As with other areas of the topic, this is presently a very active research area and our knowledge and understanding of the phenomena are growing and improving continuously. A number of excellent reviews of the field, suitable for advanced study, are listed in the bibliography.

5.6.1 Compaction of nanopowders

Problems which arise during the compaction and sintering of nanopowders may adversely influence the overall quality of the product. Generally speaking, most defects can be traced to one of several causes, including the presence of hard agglomerated particles, high plastic yield and fracture resistance, resistance to particle motion under pressure and contamination of particle surfaces. Irrespective of the consolidation method employed, the influence of each of these factors is essentially the same; they render the processes of compaction and densification more difficult.

Ideally, it would be desirable to have as starting materials for consolidation, clean, unagglomerated nanostructured powders. The powders themselves may have a micron-scale average particle size, $\langle D \rangle$, or they may be true nanopowders, depending on their synthesis route. They would be compacted at low or moderate temperature to produce a so-called green body with a density in excess of 90% of the theoretical maximum. Any residual porosity would be evenly distributed throughout the material and the pores would be fine in scale and have a narrow size distribution.

Unfortunately, most powders show some degree of deviation from this ideal. Most sintering defects can be related to the microstructures of the compacts in this 'green' state. Such defects are far more problematic when the powders are in the nanosize range than in the case for conventional powders. In particular, the elimination of pores with sizes greater than or equal to the size of the nanopowder particles is particularly troublesome. Such pores may result from the presence of particle agglomerates.

Pressing of metallic powders to produce a green body would, on the conventional (micron) scale, also involve a certain amount of plastic yielding of the particles or their fracture. The pressure required to produce a high degree of compaction is normally several times the yield stress of the material being compacted. Due to the dependence of yield stress on $\langle d \rangle^{-1/2}$ (i.e., the Hall–Petch relationship (1.23)), the cold compaction of metal nano-powders is likely to require stresses in the gigapascal (10^9 Pa) range, for which non-conventional compaction routes would be necessary.

Compaction on the conventional scale would also involve a certain amount of sliding and rearrangement, both of which become increasingly difficult as particle size decreases. On the nanoscale, the frictional force between particles becomes a very significant obstacle to their relative motion and rearrangement. These factors contribute to the formation of green bodies with a lower density than would be considered acceptable for conventional micron-scale powders.

Rearrangement of the particles may be facilitated by the use of lubricants or via wet compaction, either individually or in combination with ultrasonic agitation or centrifuging to promote good powder packing prior to pressing and/or sintering. Warm compaction methods which aim primarily to remove surface contamination and impurities also have the effect of reducing the material yield stress. Their application to the compaction of nanomaterials has also led to improvement of green body density. However, the distribution of the residual porosity still strongly depends on the state of agglomeration of the powders.

5.6.2 Sintering

Nanoscale powders are characterised by an extremely high surface area; for example, 1 kg of a copper powder in the form of spheres of radius 5 nm has a total surface area calculated using Equation (5.27) of around 75 000 m^2. If the radius were 50 μm, the surface area would be 15 m^2. Associated with this large surface area is a very substantial amount of energy, and it is this energy that drives sintering.

Sintering is a process which occurs when powders are packed together and heated to a high temperature, typically $\sim 2T_m/3$, when diffusion becomes significant. Necks begin to form at powder contact points which grow, thereby reducing the overall surface area and densifying the powder. Atoms diffuse from the grain boundaries established at intersections between differently oriented particles and deposit on the interior surface of

the pore, thereby filling up the remaining space. It is worth noting that the 'green' component will shrink during normal sintering as the porosity progressively disappears and the density increases.

The driving force for sintering is given by γ_S/r, where γ_S is the surface energy (generally considered in this type of analysis to be isotropic, but not necessarily true for nanopowders) and r is the radius of curvature of the particle (taken as the actual particle radius in unagglomerated spherical powders). The main mechanism facilitating mass transport is usually considered to be grain boundary diffusion. The assumption of isotropic surface energy is not necessarily true for nanopowders; as each particle is composed only of a limited number of atoms, they may exhibit faceting behaviour as a result. Differences in local atomic arrangement at the surface of nanoparticles, compared with the same material at a conventional particle size, may also contribute to differences in surface energy. Stabilisation of particle surfaces, such as by oxidation, will also tend to reduce the driving force for sintering. Our present understanding does not allow us to incorporate these additional influences into an analysis of sintering in a simple way.

From the argument presented so far, it is possible to infer that the rate of sintering in fine powders should be very much enhanced as a result of the reduced diffusion distances involved as well as the increased surface area. We can also infer that it will vary with temperature in a similar way to that of the diffusion coefficient. Many equations have been suggested for the rate of densification by sintering, but their general form is well represented by

$$\frac{d\rho}{dt} \propto \frac{1}{\langle D \rangle^n} \exp\left[\frac{-Q}{RT}\right], \tag{5.41}$$

where n is a constant, ρ is the density, Q is the activation energy for sintering and $\langle D \rangle$ is the mean powder particle diameter. The exponent n is typically about 3 and Q is usually considered equal to the activation energy for grain boundary diffusion.

An increased surface area such as that possessed by nanopowders should result in an enhanced densification rate at a given sintering temperature. Indeed it would suggest that full densification of a particular material should be achievable at much lower sintering temperatures. This is very attractive from the viewpoint of restricting grain growth during sintering but, as with many of our other expectations related to the nanoscale, it is unusual to observe rapid low-temperature densification in practice. This may be related to anisotropy of surface energy, as any anisotropy effect will be much more pronounced at low sintering temperatures; the surface energy becomes much more isotropic as T is increased.

5.6.3 Role of impurities

The ideal way of reducing impurities in nanopowders would seem to be to conduct all handling and compaction processes within a controlled environment. The IGC apparatus described in Section 5.3.3, for example, was designed to allow all operations, including powder formation and consolidation, to be conducted within the same chamber. In a manufacturing environment, however, powders may be consolidated at a

location remote from the powder production facility, be that as a result of cost or logistical factors, so that contamination in the form of adsorbed gases and oxide films is highly likely. Alternatively the addition of surfactants to reduce agglomeration during wet processing will also inevitably give rise to a surface layer of impurities. Because sintering is controlled by surface processes, however, the densification kinetics are highly dependent on particle surface purity and quality. In the case of the sintering of nanopowders, with their enormous surface area, this issue becomes even more critical.

The extent of particle contamination is generally speaking a strong function of the powder synthesis route. For example, powders produced by the MA route are generally considered to be more contaminated than those made by IGC, largely as a result of pick-up from the milling medium. This is not an insurmountable problem. Impurities in metallic powders produced by MA are distributed throughout the bulk of the large nanostructured powder particles rather than being concentrated solely on the surface. In the case of ceramics such as oxides and nitrides which have been milled to the nanoscale, the presence of certain contaminants may be useful in preventing grain growth if they are present as fine dispersions (Section 5.5.3).

Given their enormous specific surface area, the concentration of adsorbed gas is, perhaps unsurprisingly, much higher than for micron-scale powders. Oxygen contamination, in particular, may cause problems for sintering of metallic powders as this oxygen tends to be present in the form of a surface oxide film. The stability of the oxide is of great importance in the processing of metals as such a barrier will inhibit sintering. The presence of an oxide film may, however, be desirable from a handling viewpoint as it can reduce the risk of powder explosion on contact with air. Oxides may then be considered as desirable or undesirable, depending on the stage of processing. The ideal scenario is one where an oxide is present during powder handling and subsequently removed either before or during the consolidation step. This can be achieved by careful selection of process conditions. For example, employing a reducing atmosphere such as hydrogen during sintering, which is also commonly used in the sintering of conventional sized metal powders, leads to a reduction of the oxide and, hence, a reduction in the sintering temperature required for metallic nanopowders. Sintering metallic nanopowders in a vacuum may also reduce the required sintering temperature if the oxide breaks down under these conditions, although the effect is less pronounced than for hydrogen. Ceramic nanopowders are found to densify at lower temperatures, or to achieve greater densities at high temperatures, when sintered in a vacuum rather than in air. So the choice of sintering atmosphere would seem to be of central importance to the overall kinetics of densification.

Further improvements in densification may be possible by using novel sintering processes, such as field-activated sintering, which seems to offer a good alternative route for the processing of nanopowders in cases where very high purity products are required.

5.6.4 Porosity

As densification is effectively the removal of residual porosity, the size and spatial distribution of pores will exert a significant influence on the overall densification kinetics. If the porosity is unevenly distributed, for example as a result of the presence

of hard agglomerates in the powder, it may be impossible to achieve full, or near-full, density. The pores in this case become defects and they may significantly influence both the mechanical and physical properties of the material in which they reside. As a result care must be taken during the consolidation stage of processing to ensure that the porosity is as fine and as well distributed as possible.

Equation (5.41) can be reformulated to account for the presence of a well-dispersed low volume fraction of pores, thus

$$\frac{1}{\rho(t)(1-\rho(t))}\frac{d\rho}{dt} \propto \frac{1}{r_{\mathrm{p}}(t)}\frac{1}{\langle D\rangle^{n}}\exp\left[\frac{-Q}{RT}\right], \tag{5.42}$$

where $\rho(t)$ and $r_{\mathrm{p}}(t)$ are the instantaneous density and the instantaneous pore radius, respectively.

Equation (5.42) demonstrates that the highest sintering rates will be achieved for materials containing the finest pores. These same small pores are, however, also those responsible for the inhibition of grain boundary motion, and hence grain growth (Equations 5.38 to 5.40). As long as the rate at which the pores disappear is balanced by the rate of reduction in pore size; i.e., that the ratio $f_{\mathrm{r}}/r_{\mathrm{p}}$ remains constant, no grain growth will occur. On achieving full or near full density, however, with the restraining influence of the pores no longer operative, the rate of grain growth can be quite spectacular. This is demonstrated quite clearly in Figures 5.9 and 5.10.

5.6.5 Non-conventional processing

A number of non-conventional methods have been applied to the densification of nanopowders, including microwave sintering; shock or dynamic consolidation; and field-assisted sintering. All have been applied with the objective of enhancing densification rate, thereby allowing processing temperature and/or time to be reduced, with the ultimate aim of retaining the initial nanostructure. Of the methods listed above, the one that is currently generating most interest for the manufacture of BNMs is field-assisted sintering (FAS), sometimes referred to as spark/plasma sintering (SPS).

FAS methods involve the combination of the application of a pressure, P, and heating by the application of an electric current. In the initial stages of sintering, the multiple discharges of electrical current are passed through the powder compact. This is believed to promote the removal of surface adsorbates via generation of plasma and, hence, to enhance the process of bonding during the sintering process thus leading to a higher rate of densification. A typical FAS arrangement is shown in Figure 5.10; this press is usually contained in a chamber that allows the sintering operation to take place under vacuum or a protective gas atmosphere. The major advantage of this consolidation method is the very rapid rates of densification which may be achieved at relatively low temperatures. The cycle time from powder to component is relatively quick and the process is very attractive from the view point of commercialisation.

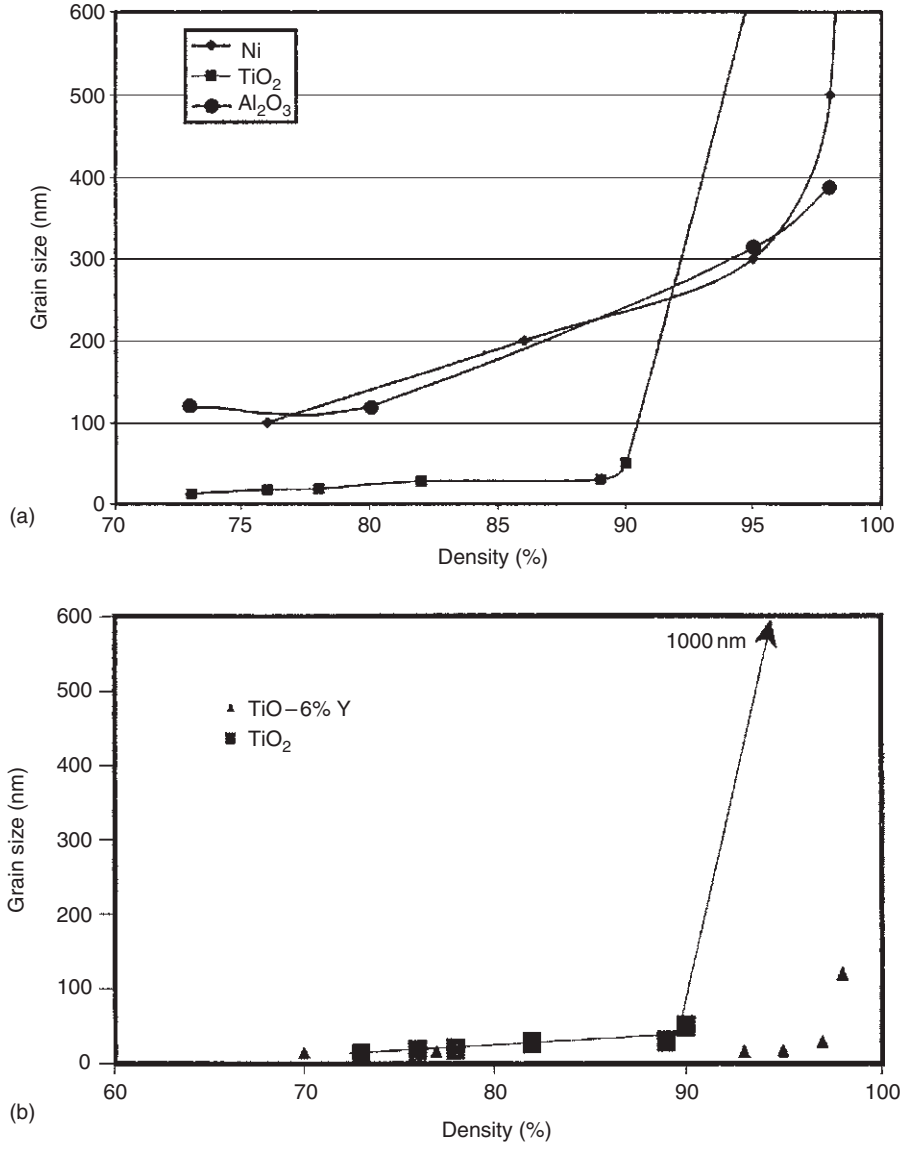

Figure 5.9 The effect of compact density on grain growth for (a) nanocrystalline Ni, TiO_2 and Al_2O_3 and (b) for TiO doped with 6% yttrium and TiO_2 showing a possible solute drag effect on grain growth. After J. Groza, Consolidation methods, in *Nanostructured Materials: Processing Properties and Applications*, ed. C. C. Koch, 2003. Reproduced by permission of IOP Publishing Limited

In terms of the types of materials that may be processed in this way to date, a variety of nanostructured pure metals, intermetallics, oxide, carbides, nitrides and composite systems have been manufactured. In all cases the nanostructure was retained after FAS was complete.

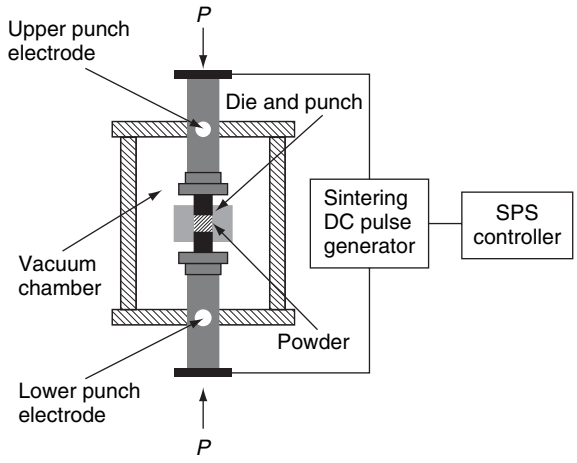

Figure 5.10 Schematic diagram of a spark/plasma sintering unit

5.7 MECHANICAL PROPERTIES

Extrapolation of mechanical properties from the conventional to the nanoscale led to an expectation amongst scientists and engineers that a significant improvement in both the strength and ductility of materials could be achieved by continued refinement of microstructural scale. In reality, however, whilst an increase in hardness and strength have been realised for nanostructured materials, the ductility is disappointingly low, showing an overall decrease when compared with materials of conventional grain size.

It would appear that when the length scale of the microstructure and the characteristic lengths relevant to deformation become comparable interesting new properties are indeed obtained. These may not, however, be quite as useful as with other cases. An extreme example is the change in mechanical behaviour of Cu from a ductile metal with moderate to low strength at conventional microstructural scales, to an extremely strong metal, with a yield strength approaching 1 GPa, but having a low (~2%) ductility, almost bordering on brittle, at grain sizes of less than 20 nm.

In this section some of the reasons for such high strengths and low ductilities are considered. As yet, there is no definitive answer to this problem and this may remain the case until defect-free BNMs become easier to manufacture reproducibly.

5.7.1 Hardness and strength

As discussed in Section 5.3.5 in connection with mechanical milling, the hardness and strength for materials of conventional grain size ($d > 1\,\mu m$) may be expressed by the empirical Hall–Petch equation (1.23). This $\langle d \rangle^{-1/2}$ dependence of the yield strength is also valid well into the nanosize range. However, it is obvious that the Hall–Petch relationship cannot be extrapolated to arbitrarily small grain sizes, and some form of lower limit to this behaviour must exist.

The pile-up model for the Hall–Petch expression requires that a large number of dislocations be present to form a dislocation pile-up. The most fundamental 'characteristic length' associated with a dislocation is the Burgers vector, **b**, which indicates the extent to which the crystal lattice is distorted by the presence of a single dislocation. There is also a further characteristic length associated with dislocation propagation; that of the equilibrium loop diameter $d(\tau)$. This is the minimum diameter that a curved dislocation line may assume under a shear stress τ, and it is given by

$$d(\tau) = \frac{Gb}{\tau}, \tag{5.43}$$

where b is the magnitude of the Burgers vector. If the shear stress is equal to that required for propagation, $\langle d \rangle$ must be at least equal to this critical length scale if deformation is to proceed by dislocation-mediated plasticity. The number of dislocations that can be contained within a grain is a function of grain size. According to the pile-up model, however, many such dislocations are required, and as the dislocation number within a grain decreases, an increasing deviation in yield strength from the plot of σ_y versus $\langle d \rangle^{-1/2}$ is to be expected. Based on this argument it has been suggested that the smallest possible 'pile-up' would consist of two dislocations and, hence, the minimum grain size for which this type of deformation mechanism would be valid would be that which could support the presence of just two dislocations. Below this, strength would be expected to remain constant or even to decrease, perhaps as a result of the dominant influence of other microstructural features. It has been proposed that as the fraction of the material associated with grain corners increases, this would produce a softening effect. Equally, it has been suggested that the increase in number of fast diffusion paths available to nanomaterials should facilitate the accommodation of deformation via grain boundary creep.

There are alternative explanations of the Hall–Petch relationship that do not depend on a dislocation pile-up mechanism. One of these alternatives suggests that ledges on grain boundaries are the source of dislocation activity (Figure 5.8(b)). The flow stress of a material is, in this case, proportional to the square root of the dislocation density, ρ_d, via the classical Taylor relationship for work hardening; i.e.,

$$\sigma_y = \alpha G b \rho_d^{1/2} \tag{5.44}$$

where α is a constant and G is the shear modulus. The dislocation density is proportional to the number of grain boundary ledges and this, in turn, is a function of the grain size. This reasoning also leads to the Hall–Petch σ_y versus $\langle d \rangle^{-1/2}$ relationship. Again this strengthening effect must be limited to a finite level as the number of boundary ledges scales with $\langle d \rangle$.

A deviation from normal behaviour would be expected for Cu at grain sizes below 20 nm in both conceptual frameworks. Experimentally, hardness data reveals a number of different material responses at grain sizes below $\sim$20 nm. These include a normal Hall–Petch behaviour, no dependence of hardness on grain size ('zero slope') and in some cases a negative slope (so-called negative Hall–Petch behaviour).

It is emphasised that most negative Hall–Petch data obtained for nanocrystalline materials has been generated using nanomaterials annealed to increase their grain size prior to testing. This has led to the suggestion that the effect could be more readily

ascribed to changes in microstructure such as densification, stress relief, phase transformation or changes in grain boundary structure rather than as a result of some underlying 'new' physical process.

5.7.2 Ductility and toughness

Studies to date indicate that there are three factors limiting the ductility of nanostructured materials: the presence of structural artefacts arising from processing, such as porosity or cracks; crack nucleation or propagation instability; plastic instability in tension.

Upon deformation, many nanomaterials are found to fracture within or only slightly beyond the elastic range. As fully dense BNMs are difficult to process, an obvious reason for this low fracture strength would be the presence of defects such as porosity or cracks or poor interparticle bonding. These may act as crack initiation sites resulting in easy crack nucleation and growth, promoting brittle behaviour in tension and causing premature failure before yielding has a chance to occur. The ductility of nanomaterials may therefore be severely compromised by their presence.

Factors other than the presence of defects may also act to limit the fracture strength and ductility of nanomaterials; for example, it is well known that grain size has a strong effect on ductility and toughness in materials of conventional grain size. In the case of nanomaterials, as the yield strength is dramatically elevated as a result of the very fine grain size, it is quite possible that it will become equal to or even exceed the fracture strength of the material. This is further exacerbated by the possibility of the fracture stress being reduced for nanoscale materials, which may arise as a consequence of the combination of reduced dislocation activity and increased grain boundary density. The high energy and the large number of these regions allow cracks to propagate along the boundaries, or intergranularly, with relative ease.

In general, there is also a tendency for nanomaterials to deform non-uniformly in tension by the production of shear bands. These are highly localised regions of material where all deformation is accommodated. As deformation proceeds, these regions become severely strained and may pull apart, leading to failure in the initial stage of straining in tension and very low apparent ductility. Once again, this may be related to the inability of nanometals to store dislocations and to uniformly work-harden, thereby sustaining the applied load without the formation of plastic instabilities.

One recently applied method of improving the ductility of nanomaterials is to manufacture materials with a bimodal grain size distribution. If large grains or dendrites are introduced into a nanomaterial matrix, either by an in situ process or by the mixing of powders of different different particle sizes prior to consolidation, these larger grains will be significantly softer than the nanostructured component during the initial stages of deformation. If the grain size of this 'soft' component is sufficiently large to allow the storage of dislocations and hence to experience work hardening, the net effect will be that, whilst the initially hard nanostructure becomes softer by the formation of shear bands, these large grains will become harder. Yield stress will therefore depend on the nanocomponent and ductility will depend on the work-hardening behaviour of these larger crystals.

Such use of widely or bimodally distributed grain sizes in structural applications is one way in which the excellent potential of high-strength nanomaterials may finally be realised, although research in this area is very much in its infancy at the time of writing (2004).

5.7.3 Creep and superplasticity

Creep is time-dependent, plastic deformation at constant stress. It occurs at all temperatures but usually becomes important only as the temperature approaches $\sim 0.5T_m$. For conventional grain sizes it has also been found to be strongly dependent on grain size. Superplasticity, on the other hand, is the ability of some polycrystalline materials to exhibit very large tensile deformations without necking or fracture. Elongations of 100% to over 1000% are typically considered as defining features of this phenomenon. In the conventional microcrystalline regime it is found that, as the grain size is decreased, the temperature at which superplasticity is observed is decreased and the strain rate at which it may occur is increased.

The generic equation for creep and superplasticity in the steady-state regime (i.e., when a stable microstructure is attained and the strain rate $\dot{\varepsilon}$ becomes constant with time) is given by an exponential law:

$$\dot{\varepsilon} = A\frac{DGb}{k_B T}\left(\frac{b}{\langle d\rangle}\right)^s\left(\frac{\sigma}{G}\right)^n, \tag{5.45}$$

where A is a constant depending on the creep mechanism, σ is the applied stress, s is the grain size exponent and n is the strain exponent. The values of the exponents s and n depend on the creep mechanism in operation, which in turn depends on the temperature and stress conditions and the initial microstructure of the material. The equation is phenomenological but is found to work well for both creep and high strain rate creep, or superplasticity. For example, for high-temperature ($\sim 0.9\,T_m$), low-stress Nabarro–Herring creep, in which deformation takes place by vacancy diffusion through the lattice, $n = 1$ and $s = 2$: for Coble creep, in which deformation is accommodated by vacancy diffusion at grain boundaries and which may occur at lower temperatures since the activation energy for grain boundary diffusion is smaller, $n = 1$ and $s = 3$. At intermediate to high stresses and temperatures between about $0.4T_m$ and $0.7T_m$, creep is governed by the movement of dislocations. Dislocation movement comprises glide along slip planes followed by climb (a diffusion-assisted process) over any obstacles encountered. Values of s and n in this intermediate regime reflect the dominance of one of these mechanisms of dislocation motion over another. When glide dominates then $n = 3$ and $s = 0$; there is no grain size dependence. When climb dominates then $n = 5$.

Superplasticity is a special case of high strain rate creep that occurs for some fine-grained materials in which grain growth is severely inhibited by the presence of a dispersion of pinning particles. As a result of the large grain boundary fraction (F_V), grain boundary sliding (GBS) becomes the predominant deformation mechanism. In this case, $n = 2$ and $s = 2$ if GBS is accommodated by dislocation movement controlled by lattice diffusion, or $n = 2$ and $s = 3$ if GBS is accommodated by dislocation movement controlled by grain boundary diffusion.

From this description of the phenomena, we might reasonably expect, at low grain sizes and low T/T_m, that Coble creep would be the dominant mechanism in nanomaterials as mass transport is dominated by grain boundary diffusion. If this were the case, enhanced creep rates, up to nine orders of magnitude greater than for the microcrystalline regime, would be expected in the case of nanomaterials. Similarly, we should also expect superplasticity to occur in nanomaterials at lower temperatures, perhaps even at room temperature, and higher strain rates than for the equivalent materials on the micron scale. In reality, echoing the observations for strength and ductility, the creep and superplastic behaviour observed for BNMs have not yet matched these predictions; the creep rate observed for a given nanomaterial is comparable to or lower than that of its coarse-grained counterpart whilst convincing evidence for superplasticity has yet to be reported for temperatures lower than $0.5T_m$. Why this should be is not yet clear, but what emerges from the scientific literature is that the investigation of these phenomena in BNMs has, in the past, been hindered by the presence of processing defects and impurities. As the processing of nanomaterials to form BNMs with controlled composition and microstructure becomes easier, their true behaviour with respect to creep and superplasticity should become clearer.

5.8 FERROMAGNETIC PROPERTIES

The properties of ferromagnetic nanomaterials are discussed fully in Chapter 4. In this section we will concentrate on the influence of material processing and defects on the properties developed. We will also look at nanocomposite magnets with remarkable soft and hard magnetic properties, examining the main structural features responsible.

5.8.1 Fundamental magnetic properties

Saturation magnetisation M_s was one of the properties of nanomaterials that were touted as showing a significant change in magnitude compared with conventional materials. Rather like the Young's modulus, early reports of a reduction of $\sim 40\%$ in saturation magnetisation M_s for consolidated nanocrystalline Fe compared with coarse-grained Fe were found, after considerable experimental and modelling effort, to result from the presence of processing defects. The initial reasoning put forward to explain the decrease, based on an enhanced degree of structural disorder in the system, resulting from a high fraction of particles within the boundary, was not well supported theoretically, and comparison of the behaviour of fully dense electrodeposited nanocrystalline nickel and fully dense coarse-grained nickel showed that there was little or no change ($<5\%$) in M_s down to grain sizes of ~ 10 nm. The presence of oxides and other impurities on the surface of nanocrystalline nickel, however, can lead to significant changes in M_s.

In the case of very small nanoparticles, for which the fraction of surface atomic sites is large, some change in the Curie temperature, T_C, compared with the values for larger grain sizes on both the nano and conventional scales may be expected. The high fraction of atoms associated with either the particle surface or the grain boundaries should in fact alter T_C. In practice, however, only small deviations from the value of T_C for the bulk have been reported up to now.

5.8.2 Nanocomposite soft magnetic materials

The structure of soft magnetic nanocomposites is of utmost importance in determining their overall properties. Their crystallisation behaviour is discussed in Section 5.3.3, where it was noted that these alloys are in fact two-phase nanocomposites. In Finemet (FeSiBNbCu) and Nanoperm (FeZrBCu) the Curie temperatures of both the nanocrystalline and amorphous intergranular phase are important in describing the magnetic response. The intergranular phase, which is typically richer in non-magnetic species, generally has a lower T_C. The soft magnetic properties of the nanocomposites are dependent on the strength of the exchange coupling between the ferromagnetic grains through this amorphous layer which, in turn, is a strong function of T. As the temperature approaches the Curie point for the amorphous layer, coercivity increases dramatically, reflecting a decrease in the exchange length, L_{ex}, as a result of the magnetic decoupling of the grains. Controlling the composition and stability of this intergranular layer is therefore of paramount importance in generating and maintaining good soft magnetic characteristics.

On the other hand, the nanocrystalline structure of FeTaC soft magnetic materials derived by devitrification of a precursor metallic glass differ significantly from that for typical FINEMET or Nanoperm compositions. In this type of alloy, a refractory carbide phase (in this case tantalum carbide) tends to form at grain boundary triple points. These carbides tend to pin grain boundaries, which prevents structural coarsening. This fully nanocrystalline structure leads to a simplification of the magnetic behaviour with respect to T. Interestingly, because of the structural scale of the carbides and the nanocrystallites, this type of structure would also seem to be a promising candidate for hard surface coatings.

5.8.3 Hard magnetic materials

Exchange spring magnets are nanocomposite structures comprising hard and soft magnetic phases that interact via magnetic exchange coupling. These two-phase mixtures can exhibit a remanence ratio M_r/M_s (where M_r is the remanent magnetisation) greater than the theoretical upper limit of 0.5 predicted by the Stoner–Wohlfarth theory, hence they are referred to as remanence-enhanced materials. Exchange coupling between the hard and soft magnetic grains that form the microstructure forces the magnetisation vector of the soft phase to be rotated parallel to easy directions of adjacent hard-phase crystallites. Because the maximum energy product of this type of hard magnet is so large, they show great promise for advanced permanent magnet applications. Significant manufacturing problems are posed by the requirement that both the hard and soft phases are nanostructured and the requirement that the structure needs a sufficient degree of coherence across the interphase boundaries to allow the grains to be exchange coupled.

Originally observed for Fe-rich hard magnetic compositions (e.g., $Fe_{78}Nd_4B_{18}$), where a low volume fraction of the hard $Nd_2Fe_{14}B$ phase was surrounded by a magnetically soft Fe_3B phase, this has since been observed in systems where the magnetically soft phase α-Fe is present and also in entirely different alloy systems such as FePt(hard)–Fe_3Pt (soft).

Preparation has generally been via more conventional non-equilibrium processes such as melt spinning, either to form the desired structure directly or by devitrification of an amorphous precursor, or mechanical milling. More recently, however, FePt–Fe_3Pt

exchange spring magnets have been produced by sintering self-assembled mixtures of nanopowder precursors (FePt and Fe_3O_4) in a reducing atmosphere. The advantage of this method is that any relative combination of the two phases may be produced without the need for a suitable glass-forming composition being available. Thus, the magnetic properties can be engineered with great precision.

5.9 CATALYTIC PROPERTIES

The very high, very controllable, reactive surface area of nanopowders renders them ideal for use as catalysts; in fact, during the 1970s this was one of their first real applications. The properties of nanocatalysts may be explained, generally speaking, by simply extending well-known relationships for the sensitivity of catalytic activity and the selectivity to particle size into the nano range. There are exceptions, such as the much enhanced efficiency of ultrafine (below 6 nm) nanoparticles of Pt in the catalytic reduction of NO_2, and the enhanced catalytic activity of rutile (TiO_2) nanoparticles associated with the oxygen-deficient compositions which may exist as a result of processing. Hydrogen-absorbing alloys also show improved sorption properties over their coarse-grained counterparts. Enhanced surface diffusion also plays a role, particularly for gas sensor sensitivity and in hydrogen storage applications.

5.10 PRESENT AND POTENTIAL APPLICATIONS FOR NANOMATERIALS

Nanomaterials are relatively new developments and have received significant attention only during the past one or two decades. The number of existing applications for nanomaterials is therefore quite small. Those industries currently using nanomaterials range from the more obvious (e.g., the magnetics industry), to the surprising (e.g., the cosmetics industry). In fact, the cosmetics industry was one of the first to see the potential of nanomaterials and an interesting example is described below. There is potential for wider use in the production of coatings with tailored moduli and some possible applications are briefly discussed. If and when the mechanical properties of BNMs become more reproducible and problems associated with ductility and toughness are addressed nanomaterials should find niche markets in these applications also, but the present examples will concentrate on the most probable fields of application.

5.10.1 Ultraviolet absorbers

The cosmetics industry has used nanomaterials for some time. A particularly interesting example is the use of semiconducting oxide ceramics as UV absorbers or sunscreens. The conflicting issues of cosmetic appeal and UV absorption efficiency make conventionally sized oxide powders unsuitable because they impart excessive whitening to the skin upon application, although they offer effective UV protection for much longer than the competing organic-based screens.

The degrees of diffuse and specular reflection and scattering that are largely responsible for the whitening effect may be significantly reduced by using a nano-powder with a suitable particle diameter $\langle D \rangle$. On length scales small in comparison with the wavelength of incident light, scattering shows a sixth-power dependence on particle size, indicating that a relatively small reduction in average particle size and close control of the PSD will lead to a significant decrease in intensity of scattered light and therefore whiteness.

The refractive index and band gap of the ceramic component are also of great importance for good performance. Low values of the refractive index are necessary, as is absorption of light over the widest possible range of the UV part of the spectra. The oxide semiconductors ZnO and TiO_2, which have both low refractive indices and suitable band gap energies corresponding to wavelengths of $\sim$380 and $\sim$365 nm, respectively, are prime candidates for this role.

Unless $\langle D \rangle$ becomes sufficiently small that it begins to exhibit quantum dot behaviour; i.e., if the particles become smaller than the exciton Bohr diameter ($\sim$5 nm for both ZnO and TiO_2), where the band gap will become smaller and the UV absorption efficiency will be compromised; there is no size effect on absorption efficiency. Optimisation of $\langle D \rangle$ and PSD are driven by the need to compromise between protection via UV absorption and reflection mechanisms.

5.10.2 Magnetic applications

There are a number of exciting developments in magnetic materials that are dependent on materials possessing nanoscale microstructures. In particular, ultrasoft nanocomposite magnets and exchange-enhanced permanent magnets have been a key driving force the behind developments in the whole of the inorganic nanomaterials field.

The extremely soft magnetic properties and low cost of the new nanocomposite and nanocrystalline Fe-based magnetic alloys are being exploited in power electronics applications and for earth leakage devices, with further potential applications in magnetic shielding and sensors. The material producers and the method of production are so similar to those used in the manufacture of amorphous ferromagnetic alloys that these materials have already found some niche applications.

The market for exchange-enhanced nanocrystalline magnets is potentially very large. Bonded rare earth magnets are increasingly used in motors and actuators in many consumer products, and increasing their maximum energy product will enable the manufacture of smaller components with the same functionality. Flexibility of manufacture and the ability to tailor properties to specific applications are further enticements for manufacturers to utilize them.

5.10.3 Coatings

There is presently considerable interest in the development of nanostructured and nanolayered coatings. The methods used in their production (e.g., plasma-assisted vacuum techniques) make it is possible to synthesise materials with extreme mechanical

properties that would be difficult by other means. The formation of coatings with ultra-high hardness and an associated high elastic modulus has been the target of much R&D activity in this area. This is largely because conventional fracture mechanics theory suggests this as a development vector and also that these properties are desirable for improving tribological properties. There is an alternative approach that has not yet been widely investigated – nanocomposite coatings with high hardness and *low* elastic moduli. These coatings may exhibit improved toughness and may therefore be better suited for optimising the wear resistance of 'real' industrial substrate materials, such as steels and light alloys, by providing a better modulus match. These nanocomposite coatings, although not necessarily exhibiting extreme hardness, may also provide superior wear resistance when deposited on the types of substrate material employed by industry.

Good examples of this type of coating are in the TiAlBN system for which the Al content appears to govern the elastic modulus; chromium nitride and tungsten carbide formed by 'doping' of elemental metallic systems also seem to offer promise. Thermal barrier coatings also appear to be particular candidates for nanostructured coatings.

BIBLIOGRAPHY

General overview

M. F. Ashby and D. R. H. Jones, *Engineering Materials*, Vols 1 and 2, Pergamon Press, New York, 1980, 1986.

J. C. Anderson, K. D. Leaver, R. D. Rawlings and J. M. Alexander, *Materials Science*, Van Nostrand Reinhold, London, 1987

Thermodynamics and kinetics

J. W. Martin, R. D. Doherty and B. Cantor, *Stability of Microstructure in Metallic Systems*, Cambridge University Press, Cambridge, 1997.

D. A. Porter and K. E. Easterling, *Phase Transformations in Metals and Alloys*, 2nd edn, Van Nostrand Reinhold, London, 1992.

J. W. Christian, *The Theory of Transformations in Metals and Alloys*, 1st edn, Pergamon Press, 1965.

The first two are also good sources of information on the stability of microstructures.

Synthesis

I. Brodie and J. J. Murray, *The Physics of Micro/Nano Fabrication*, Plenum Press, New York, 1992.

C. Surayanarayana (ed.), *Non-Equilibrium Processing of Materials*, Pergamon, Oxford, 1999.

C. Koch (ed.), *Nanostructured Materials: Processing, Properties and Potential Applications*, William Andrew Publishing, New York, 2002.

Stability

D. S. Wilkinson, *Mass Transport in Solids and Fluids*, Cambridge University Press, Cambridge, 2000.
F. J. Humphreys, *Recrystallization and Related Annealing Phenomena*, Elsevier, Oxford, 1996.
See also the first two references under 'Thermodynamics and Kinetics'.

Consolidation

J. Groza, in C. Koch (ed.), *Nanostructured Materials: Processing, Properties and Potential Applications*, William Andrew Publishing, New York, 2002.

Mechanical properties

D. G. Morris, *Mechanical Behaviour of Nanostructured Materials*, Trans Tech, Switzerland, 1998.

Magnetic properties

M. E. Mchenry, M. A. Willard and D. E. Laughlin, *Progress in Materials Science*, Vol. 44, 1999, pp. 291–433.